An analytical model to predict the temperature in subway-tunnels by coupling thermal mass and ventilation

Manuscript revised to Journal of Building Engineering: Apr. 2021

An analytical model to predict the temperature in subway-tunnels by coupling thermal mass and ventilation

Tingting Sun[a,b], Zhiwen Luo[b,] *, Tim Chay

[a] School of Building Services Science and Engineering, Xi'an University of Architecture and Technology, 710000 Xi'an, China,

[b] School of the Built Environment, University of Reading, Reading, RG6 6AY Berkshire, United Kingdom,

***Corresponding author:**

Dr. Zhiwen Luo, School of the Built Environment, University of Reading, United Kingdom

Tel: Email: z.luo@reading.ac.uk

Abstract

There is an increasing incidence of overheating in subway tunnels in recent years especially in old subways without air-conditioning e.g., London Underground. There is still lack of a clear understanding how tunnel-air temperature is determined by the complex thermal processes in subway tunnels. In this study, a mathematical model that describes the thermal processes in deeply buried subway tunnels was developed. Analytical solution was derived by separating the solution into time-averaged component and periodic component. The results show that the time-averaged component of tunnel-air temperature will approach steady state as the time tends to infinity, which has a positive linear relation with internal heat-source and average ambient temperature. Active cooling or heat-recovery systems could soon become a necessity in subway tunnels due to both global warming and increasing internal heat generation. Compared with outdoor air, the amplitude of the tunnel-air temperature shows a significant reduction in the day period but not in the year period. The surrounding soil temperature will keep changing for thousands of years. This study offers a new physical insight to analyse and mitigate overheating in subway tunnels.

Keywords: Subway tunnels; Heat transfer; Thermal mass; Ventilation; Thermal coupling

Nomenclature

A	tunnel-wall surface area for unit length tunnel, m^2/m
a_s	thermal diffusivity of soil, m^2/s
Bi	Biot number
C	specific heat, J/kg·℃
D	ratio of the time scale for ventilation that affects tunnel-air temperature and the period time length
E	internal heat source of unit length tunnel, W/m
E_{sur}	heat flux through the tunnel-wall surface of unit length tunnel, W/m
f	attenuation ratio of amplitudes of temperature
Fo	Fourier number
Fo_{R}^{ω}	Fourier number with the characteristic length of R and the characteristic time of $1/\omega$
h	convective heat transfer coefficient at the tunnel-wall surface, $W/m^2\cdot$℃
J_0, J_1	Bessel functions of the first kind with the integer 0 and 1
K_s	thermal conductivity of soil, W/m·℃
n	ventilation air change rate, ach/h(ach/s)
q	ventilation air flow rate for unit length tunnel, $m^3/(s\cdot m)$
R	hydraulic radius of the tunnel, m
r	distance from the central axle of the tunnel, m
T	temperature, ℃
t	time, s
T_E	air temperature increase due to the internal heat source E, ℃
T_g	initial soil temperature in deep ground without disturbance, ℃
u	integrable variable with the dimension of length, m
V	inner volume of unit length tunnel, m^3/m
ΔX	amplitude of X
$\Delta\tilde{X}$	transient value of periodic component of X
$\bar{X}$	time-averaged component of X
$Y0$, $Y1$	Bessel functions of the second kind with the integer 0 and 1
I_0, I_1	Modified Bessel functions of the first kind with the integer 0 and 1
K_0, K_1	Modified Bessel functions of the second kind with the integer 0 and 1
z	dimensionless distance from the central axle of the tunnel

Greek symbols

ϕ	phase shift, rad
λ	convective heat-transfer number
η_s	time-averaged heat-diffusion ratio through surrounding soil
$\Delta\eta_s$	dimensionless heat-flux amplitude at the tunnel-wall surface
Θ	the variable of θ after the Laplace transform in a complex field
θ	excess-temperature relative to T_g, ℃
ρ	density, kg/m^3
ω	frequency of outdoor-temperature fluctuation, 1/s

Subscripts

a	air
s	soil
out	outdoor
in	indoor

sur	tunnel-wall surface
∞	the value when $t \rightarrow \infty$, ℃

1. Introduction

The number of subway systems increased globally in the last few decades thanks to their high passenger-capacity and low operating-cost. As of December 2019, 188 cities in 56 countries around the world use approximately 192 subway systems [1,2]. The total system-length is over 16377 km, and the number of annual passengers exceeds 65620 million [1,2]. Unfortunately, with climate warming many of these subway systems suffer from overheating in summer - especially older systems, where air-conditioning systems are not installed [3-6]. The air temperature in the London Underground often reaches 30℃ in summer [7], with in-train temperatures of up to 41℃ [8,9]. During the 2006 European heatwave, temperatures as high as 47℃ were recorded [10]. Overheating also occurred in the subways in Tokyo, Osaka, and New York [11]. Surprisingly, a very high temperature (53℃) was recorded in the Wuhan underground (China) [11]. Such high tunnel-air temperature has a significant impact on the environment and the energy consumption (air-conditioning) in trains and subway stations [9,12,13]. To solve the overheating problem in subway tunnels, it is essential to predict the tunnel-air temperature and understand the influential factors and their interactions.

There are many tools developed to predict tunnel-air temperature, and they can be classified into two categories: commercial tools and self-built models. The commercial tools include SES [14,15], IDA Tunnel [16], CFD [15,17, 18], and STEES [9,14]. SES uses a 1-dimensional quasi-steady heat-transfer model that only outputs the maximum/minimum/average temperatures for the hottest month in the long term. The detailed temporal temperature distribution is not considered [14]. IDA Tunnel, which is based on the same basic equations and concepts as SES [16], has similar limitations. STESS could output hourly temperatures, which represents some improvement over SES [14]. However,

none of the above commercial tools enable an intuitive identification of the important parameters that affect tunnel-air temperature, which limits the exploration and assessment of the methods to solve overheating problem in subway tunnels. Among self-built models, few studies focused on the mathematical models that describe the thermal processes in subway tunnels [19,20]. Related mathematical models, however, can be found in studies of tunnels used for other purposes, such as earth-to-air heat exchangers [21-23], underground ventilation-tunnels for underground hydro-power stations [24], and railway tunnels through hills [25]. All these models considered the unsteady heat-transfer process through surrounding soil and the Robin condition at the tunnel-wall surface. Among these studies, [21] employed a 1-dimensional model to explore the effect of an earth-to-air heat exchanger on indoor thermal comfort and energy-saving effects in a typical building. A significant difference between an earth-to-air heat exchanger and a subway tunnel is that there is no internal heat source in the earth-to-air heat exchanger, which simplifies the energy-balance equation to describe the air in the tunnel. Liu [24] also proposed a 1-dimensional model, without an internal heat source, for the underground ventilation tunnel of a hydro-power station. This model was solved numerically, using the finite-difference method, to determine the variation of the tunnel-air temperature as a function of the tunnel length. Zhou [25] proposed a 2-dimensional model, which took into account the internal heat source, to study the freeze-distance at the entrance of the railway tunnel through a hill in cold regions. Using the finite difference method, a numerical solution was obtained, which can describe how the freeze-distance depends on the outdoor temperature and the wind speed in the tunnel. Another model, which also considers the internal heat source and focuses on subway tunnels, was developed by Zhang et al. [19]. The Green function was used to find analytical solution to the equations. However, a numerical solution, which uses the finite element method, was proposed later (instead of using the exact formulas for an analytical solution). The results of

this study also focused on the prediction of the inner tunnel-wall temperature (instead of the factors that influence the tunnel-air temperature or the interactions of the relevant thermal processes). Additionally, Yuan et al. [26] proposed a 1-dimensional model for an underground refuge chamber. In this model, both the heat conduction equation and the Robin condition at the tunnel-wall surface are applicable for subway tunnels. However, the two assumptions (I: The inner air-temperature is independent of time and already known. II: The distance from the tunnel centre to the remote constant-temperature boundary is a finite constant and already known) are not suitable for subway tunnels. In other words, the governing equations for subway tunnels are more complex and the corresponding solution-seeking method is very different from Yuan's model [26]. However, none of the models above provided sufficient scientific insight for tunnel-air temperature prediction and overheating mitigation effectiveness in the tunnel environment

Although few previous studies focused on the main factors that influence the tunnel-air temperature and the interdependence among the relevant thermal processes in subway tunnels [9], much research has been done to reveal the indoor-air temperature influential factors and the thermal processes in buildings [27-32]. Li [27-30] and Ma [31, 32] et.al researched the effect of internal heat sources, ventilation, thermal mass, and heat transfer on the indoor-air temperature in simplified buildings. The thermal processes in buildings are similar in subway tunnels in some ways, however, the physical model, governing equations, and boundary conditions differ significantly because the surrounding soil is (assumed) infinite for deep-buried tunnels, whereas the envelope and thermal mass of a building is of finite size. Hence, the results, which were generated from buildings, cannot be used for subway tunnels directly. Zhang and Li [9] studied the relationship between the maximum tunnel-air temperature and some influencing factors. However, there is no evidence that *all* main factors were

considered. After all, ventilation was not considered at all. Additionally, statistical methods were used in this study, which substantially weakens a study of thermal processes.

By learning from the thermal mass and ventilation study in buildings, this paper aims to apply the analytical model developed for buildings [27-30] into the tunnel environment to provide further insight on the tunnel-air prediction and overheating mitigation. Figure 1 shows the flowchart for the present study. An ideal physical/mathematical model for subway tunnels is firstly developed in this study. The governing equations are solved by separating the solutions to the time-averaged component from the periodic component. The influential factors of the tunnel-air temperature, tunnel-wall surface temperature, surrounding-soil temperature, and the heat flux through the tunnel-wall surface will be discussed. The model is also applied into London Underground to understand how overheating in London underground conditions is affected by increasing internal heat source and global warming. Finally, the solutions to cool down tunnel-air are discussed, which provides guidance for improved subway-tunnel design and operation to avoid overheating.

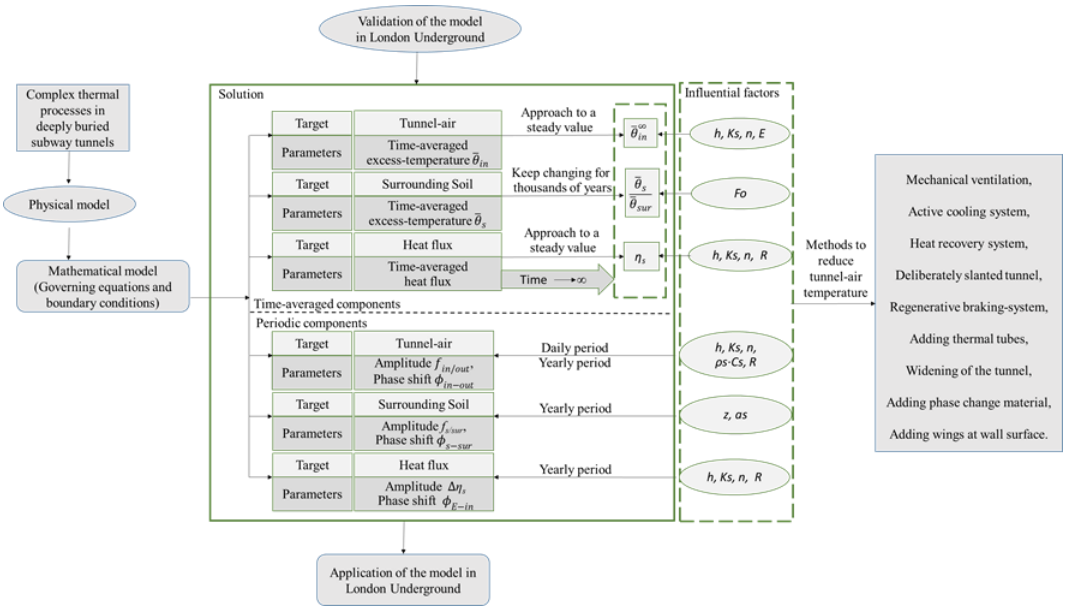

Fig.1 Flowchart of the research approach

2. Methodology

2.1 Physical model and assumptions

The structure of the subway tunnel is shown in Fig. 1. It consists of a tunnel tube, surrounding soil, and air shafts. Trains travel through the tunnel tube and generate waste heat, which represents the internal heat source in the analytical model. The waste heat is eliminated via ventilation through the air shafts as well as the heat transfer through the tunnel-wall surface and the surrounding soil. Based on this subway-tunnel model the following assumptions are made:

(1) The subway tunnel is buried deep in soil. The cross section of the subway tunnel is circular [21,24,33], and the radius is uniform everywhere.

(2) The air-temperature distribution in the tunnel is uniform, which means that the airflow is fully homogenous and the surface temperature of the tunnel wall is uniform. According to [13], the temperature distribution within a subway tunnel is not sensitive to the length of tunnel, thus this assumption is reasonable.

(3) Soil temperature only changes in the radial direction. This means that heat flow occurs only in the radial direction - not in the axial [13] or angular direction [21,22,24].

(4) The ventilation flow rate (q), internal heat source (E), and convective heat-transfer coefficient at the tunnel-wall surface (h) are assumed to be constant. For a long period, such as a day or a year, using average values of these parameters is precise enough to obtain accurate results [34].

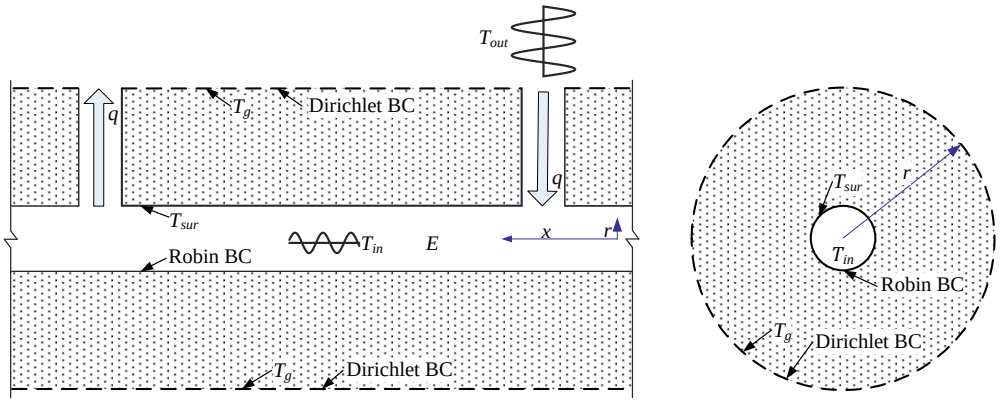

Fig. 2. An ideal subway-tunnel model with constant internal heat source and ventilation flow rate. Heat transfer through the surrounding soil only occurs in the direction of *r*.

2.2 Governing equations and boundary conditions

One-dimensional unsteady heat-transfer model is adopted considering the heat-conduction through surrounding soil. The cylindrical coordinate system is used to fit the structure of the ideal subway tunnel. The radial heat conduction can be expressed as [35]:

$$\frac{\partial T_s}{\partial t} = \frac{a_s}{r}\left(r\frac{\partial^2 T_s}{\partial r^2} + \frac{\partial T_s}{\partial r}\right) \qquad (1)$$

with the boundary conditions for Robin BC at the tunnel-wall surface and the Dirichlet BC at the distant boundary [35]:

$$-K_s \frac{\partial T_s}{\partial r}\Big|_{sur} = h(T_{in} - T_{sur}) \qquad r = R \qquad (2)$$

$$T_s(\infty, t) = T_g \qquad r = \infty \qquad (3)$$

and the initial conditions [36]:

$$T_s(r, t) = T_g \qquad r \geq R,\ t = 0 \qquad (4)$$

$$T_{in}(t) = T_g \qquad t = 0 \qquad (5)$$

Here, T_s is the temperature of the surrounding soil, ℃; t is the time, s; $a_s = \frac{K_s}{\rho_s C_s}$ is the thermal diffusivity of the soil, m^2/s; ρ_s is the soil density, kg/m^3; C_s is the specific heat of the soil, kJ/kg·℃; K_s is the soil's thermal conductivity, W/m·℃; r is the distance from the central axle of the tunnel, m; T_{sur} is the tunnel-wall surface temperature, ℃; h is the convective heat-

transfer coefficient at the tunnel-wall surface, W/m^2·℃; T_{in} is the tunnel-air temperature, ℃; T_g is the initial soil-temperature in deep ground without disturbance, ℃.

The heat balance for the air in the tunnel is [34]:

$$\rho_a C_a n\pi R^2 (T_{out} - T_{in}) + E - 2\pi Rh(T_{in} - T_{sur}) = \rho_a C_a \pi R^2 \frac{dT_{in}}{dt} \quad (6)$$

Here, ρ_a is the air density, kg/m^3; C_a is the specific heat of air, kJ/kg·℃; n is the ventilation change rate for air, ach/s; R is the tunnel radius, m; E is the internal heat source in the tunnel, W/m.

According to [27], the outdoor temperature T_{out} can be expressed as:

$$T_{out} = \bar{T}_{out} + \Delta\tilde{T}_{out} = \bar{T}_{out} + \Delta T_{out}\cos(\omega t) \quad (7)$$

Here, $\bar{T}_{out}$ and ΔT_{out} are independent of time and $\Delta T_{out} \geq 0$. ω is the frequency of the outdoor temperature fluctuation with the value 2π/(24x3600) s^{-1}, for the daily period, or 2π/(365x24x3600) s^{-1}, for the yearly period.

3 Analytical solutions

It is expected that the solutions can be expressed as $T_{in} = \bar{T}_{in} + \Delta\tilde{T}_{in} = \bar{T}_{in} + \Delta T_{in}\cos(\omega t - \phi_{in})$, $T_{sur} = \bar{T}_{sur} + \Delta\tilde{T}_{sur} = \bar{T}_{sur} + \Delta T_{sur}\cos(\omega t - \phi_{sur})$, and $T_s = \bar{T}_s + \Delta\tilde{T}_s = \bar{T}_s + \Delta T_s\cos(\omega t - \phi_s)$; i.e. they comprise time-averaged (non-periodic) components and the periodic components.

3.1 Solution for the time-averaged components

3.1.1 The time-averaged tunnel-air excess-temperature

The time-averaged tunnel-air excess-temperature ($\bar{\theta}_{in}$) may be obtained by using a Laplace transform, considering the boundary and initial conditions, and applying the inverse Laplace transform (see Appendix A):

$$\bar{\theta}_{in} = \bar{T}_{in}(t) - T_g = \frac{2}{\pi}(\bar{T}_0 + T_E - T_g)\int_0^\infty \frac{e^{-(uR)^2 Fo} - 1}{u} g(uR)du \quad (8)$$

193 where $T_E = \frac{E}{\rho_a q C_a}$,

194 $$g(uR) = \frac{g_2(uR)\left[\frac{uR}{Bi}J_1(uR)+J_0(uR)\right]-g_1(u)\left[\frac{uR}{Bi}Y_1(uR)+Y_0(uR)\right]}{g_1(u)^2+g_2(u)^2},$$

195 $$g_1(uR) = \frac{uR}{Bi}\cdot[1+\lambda-\left(\frac{R^2}{a_s}\right)^{-1}\cdot\frac{V}{q}\cdot(uR)^2]\cdot J_1(uR)+[1-\left(\frac{R^2}{a_s}\right)^{-1}\cdot\frac{V}{q}\cdot(uR)^2]\cdot J_0(uR),$$

196 $$g_2(uR) = \frac{uR}{Bi}\cdot[1+\lambda-\left(\frac{R^2}{a_s}\right)^{-1}\cdot\frac{V}{q}\cdot(uR)^2]\cdot Y_1(uR)+[1-\left(\frac{R^2}{a_s}\right)^{-1}\cdot\frac{V}{q}\cdot(uR)^2]\cdot Y_0(uR),$$

197 where u is an integrable variable with the dimension of length, m; $q = nV$ is the ventilation
198 flow rate for a unit tunnel-length, m^3/(s·m); $V = \pi R^2$ is the inner volume of unit tunnel-length,
199 m^3/m; $Fo = \frac{a_s t}{R^2}$, $Bi = \frac{hR}{K_s}$, $\lambda = \frac{hA}{\rho_a q C_a}$; $A = 2\pi R$ is the tunnel-wall surface area for one unit
200 tunnel-length, m^2/m; J_0 and J_1 are the Bessel functions of the first kind with the integers 0 and
201 1; Y_0 and Y_1 are the Bessel functions of the second kind with the integers 0 and 1. *Fo* (Fourier
202 number) is the dimensionless time, which represent the ratio of the thermal diffusion rate to
203 the thermal storage rate. *Bi* (Biot number) is used to measure the ratio of the thermal
204 resistance of the heat conduction through the soil to the thermal resistance of the convective
205 heat-transfer at the tunnel-wall surface. Yam et al. [27] introduced λ (convective heat-transfer
206 number) to measure the relative strength of the convective heat-transfer at the thermal mass
207 surface. The expressions $\frac{R^2}{a_s}$ and $\frac{V}{q}$, with a time dimension, were introduced by Holford et al.
208 [37]. The expression $\frac{R^2}{a_s}$ is used to measure the time scale needed for thermal diffusion to alter
209 mass temperature, while $\frac{V}{q}$ represents the time scale for ventilation to change the interior air-
210 temperature. Thus, $\left(\frac{R^2}{a_s}\right)^{-1}\cdot\frac{V}{q}$ describes the ratio between the two time-scales.

211 Clearly, the influencing factors for the time-averaged tunnel-air excess-temperature $\bar{\theta}_{in}$ are
212 n, E, K_s, ρ_s, C_s, h, R, ρ_a, C_a, and t. Among these, ρ_a and C_a can be assumed as constants. In
213 addition, the calculation indicates that changing the tunnel radius R matters very little for

1.4m<R<4m. This implies that $\bar{\theta}_{in}$ is mainly affected by ventilation (n), the internal heat source (E), conductive heat-transfer through surrounding soil (K_s,), heat storage by surrounding soil (ρ_s, C_s), and convective heat-transfer at the tunnel-wall surface (h).

3.1.2 The time-averaged excess-temperature of the surrounding soil

Appendix A shows the following solutions:

$$\bar{\theta}_s(t,r) = \bar{T}_s - T_g = \frac{2}{\pi}(\bar{T}_0 + T_E - T_g)\int_0^{\infty} \frac{e^{-(uR)^2 Fo}-1}{u} j(uR,ur)du \quad (9)$$

$$\bar{\theta}_{sur} = \bar{\theta}_s(t,R) = \frac{2}{\pi}(\bar{T}_0 + T_E - T_g)\int_0^{\infty} \frac{e^{-(uR)^2 Fo}-1}{u} j(uR,uR)du \quad (10)$$

Here, $j(uR,ur) = \frac{g_2(uR)J_0(ur)-g_1(uR)Y_0(ur)}{{g_1}^2(uR)+{g_2}^2(uR)}$,

$\bar{\theta}_s$ is the time-averaged surrounding-soil excess-temperature, ℃; $\bar{\theta}_{sur}$ is the time-averaged wall-surface excess-temperature, ℃. Fig. 2 shows the dimensionless surrounding soil excess-temperature $\frac{\bar{\theta}_s}{\bar{\theta}_{sur}}$ as a function of ln(r/R) and Fo. Clearly, the soil temperature stabilizes much slower than the tunnel-air temperature which stabilizes within few years [9]. There are two reasons for this: First, because soil is a poor heat-conductor, the heat diffusion occurs very slowly through the soil. Second, the surrounding soil layer is very thick. Hence, it will take a long time to obtain a reliable soil-temperature profile. Fig. 2 also indicates that the soil-temperature increase will last for a substantial amount of time. Even 7000 years later ($Fo\approx$ 10000), the soil-temperature distribution is still very different from the one theoretically reached after infinite time. For the London underground, for example, $Fo\approx$200. This suggests that the soil temperature for the London underground will continue to increase for thousand years. However, the increase will slow down. Moreover, Equation (9) provides a temperature-prediction tool for the soil surrounding subway tunnels. This tool can be used as a reference for the design of ground-source heat-pump systems near subway tunnels [38, 39]. In addition, this temperature-prediction tool can also help to analyse the stability of concrete

underground-tunnels under uneven temperature distribution [40] and the impact of heat sources from subway tunnels on urban ground temperature elevation on a city-scale [41].

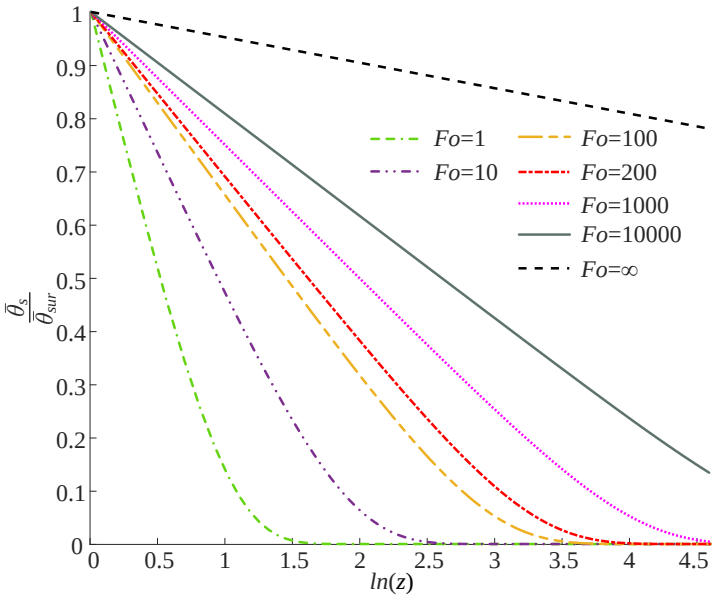

Fig. 2. The dimensionless excess-temperature of the surrounding soil as a function of ln(z) (z=r/R) and Fo (time-averaged component). The used parameters are: E=300W/m, n=15 ach/h, h=44 W/m^2·℃, K_s=0.35 W/m·℃, ρ_s =1500 kg/m^3, C_s =1842 J/kg·℃, R=1.7m, $\bar{T}_0 = T_g$ =10.3℃. The values of h, K_s, ρ_s, C_s, R, and $\bar{T}_0$ are based on the conditions in a London underground [35]. Unless stated otherwise, these are also valid for all following figures.

3.1.3 Solutions of the time-averaged components for $t \to \infty$

When $t \to \infty$, the solutions of the time-averaged components can be expressed as (see Appendix B):

$$\bar{\theta}_{sur}^{\infty} = \frac{8Bi}{8Bi+3\lambda+3}(\bar{T}_0 + T_E - T_g) \quad (11)$$

$$\bar{\theta}_{in}^{\infty} = \frac{(8Bi+3)}{8Bi+3\lambda+3}(\bar{T}_0 + T_E - T_g) \quad (12)$$

Here, z=r/R∈ [1, ∞). Using Equations (11) and (12), we can write

$$\bar{\theta}_{in}^{\infty} - \bar{\theta}_{sur}^{\infty} = \frac{3}{8Bi+3(1+\lambda)}(\bar{T}_0 + T_E - T_g) \quad (13)$$

Fig. 3 illustrates the time-averaged excess-temperature of tunnel-air for $t \to \infty$ ($\bar{\theta}_{in}^{\infty}$) as a function of h, K_s, n, and E. Fig. 3(a) suggests that, when h is very low (h<1W/m^2℃), $\bar{\theta}_{in}^{\infty}$ decreases sharply with increasing h. However, when h>5W/m^2·℃, $\bar{\theta}_{in}^{\infty}$ hardly changes. This is because the thermal resistance, which is caused by convective heat-transfer at the wall-surface, is the essential component when h is extremely low. Conversely, when h is high enough, the essential component of the thermal resistance is caused by conductive heat-transfer (instead of convective heat-transfer). As reported in previous studies, the h at tunnel-wall surface is much higher than 5W/m^2·℃ [35]. Therefore, it does make no sense to try reducing the tunnel-air temperature by enhancing convective heat-transfer. Fig. 3(b) shows how $\bar{\theta}_{in}^{\infty}$ changes with K_s. Consistent with the trend reported by Ampofo et.al. [42], $\bar{\theta}_{in}^{\infty}$ drops first sharply and then more moderately as K_s increases. As shown in Fig. 3(b), $\bar{\theta}_{in}^{\infty}$ can be reduced by about 4.5 ℃ when K_s increases from 0 to 50 W/m·℃. However, $\bar{\theta}_{in}^{\infty}$ would decrease slightly if the increase in K_s was to continue. Additionally, the increase in K_s can be obtained by adding heat pipes to the surrounding soil - see Ref. [8,43,44]. Fig. 3(c) shows the effect of the air change rate n. An extremely low n can result in a very high $\bar{\theta}_{in}^{\infty}$. The value of $\bar{\theta}_{in}^{\infty}$ decreases as n increases. The biggest change, however, occurs for the area with n<5 ach/h. The detailed view indicates that the cooling effect increases very little when n>15 ach/h. Fig. 3(d) shows a linear relationship between $\bar{\theta}_{in}^{\infty}$ and the internal heat source E, which means that it is a suitable method to reduce tunnel-air temperature by cutting down E. The methods to reduce E include the reduction of both train-weight and speed [45,46], modifying the regenerative braking-system [9], active tunnel-cooling [8,46], and waste-heat recovery from tunnels [47,48].

Fig. 3 also shows that $\bar{\theta}_{in}^{\infty} - \bar{\theta}_{sur}^{\infty}$ is very small unless h is extremely low. The value for h in the subway tunnel was reported as 44 W/ m^2·℃ [35]. This implies that there is a small

average-temperature difference between the tunnel-air and the tunnel-wall surface. Thus, the operation temperature can be assumed to be the same as the tunnel-air temperature. Moreover, it would be unwise to obtain a lower tunnel-wall surface temperature by reducing h because this would impede the heat diffusion into the soil and cause an even higher tunnel-air temperature.

Equations (11) and (12) provides a simple way to predict the air temperature and wall-surface temperature in subway tunnels. Compared with traditional methods, such as numerical methods or softwares mentioned in Section I Introduction, this developed mathematical model is time-saveing and shows the mathematical relation between tunnel-temperatures and each influencing factor clearly.

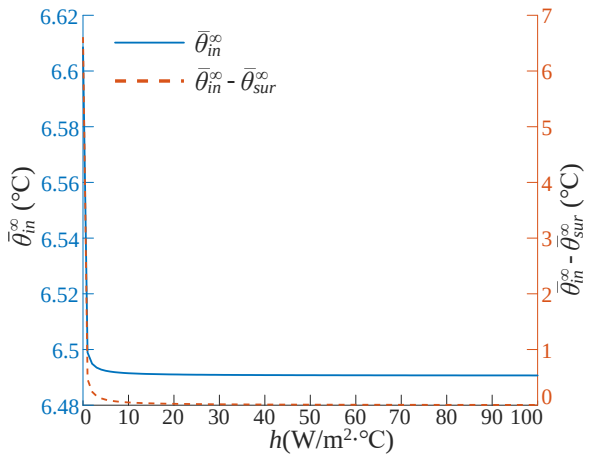

(a) $\bar{\theta}_{in}^{\infty}$ and $\bar{\theta}_{in}^{\infty} - \bar{\theta}_{sur}^{\infty}$ as a function of h

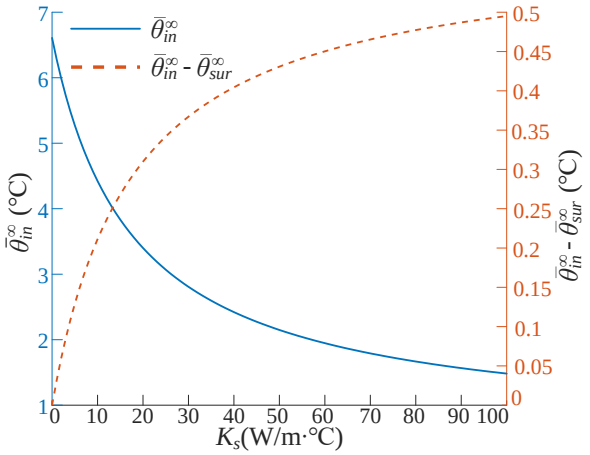

(b) $\bar{\theta}_{in}^{\infty}$ and $\bar{\theta}_{in}^{\infty} - \bar{\theta}_{sur}^{\infty}$ as a function of K_s

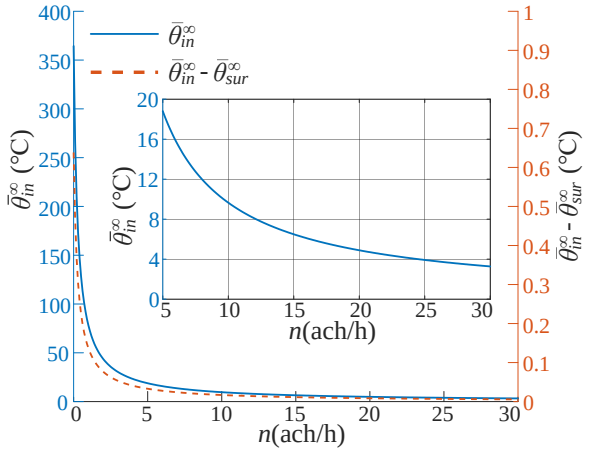

(c) $\bar{\theta}_{in}^{\infty}$ and $\bar{\theta}_{in}^{\infty} - \bar{\theta}_{sur}^{\infty}$ as a function of n

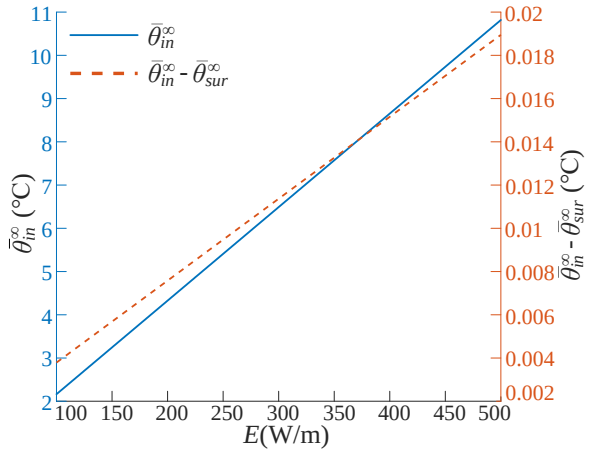

(d) $\bar{\theta}_{in}^{\infty}$ and $\bar{\theta}_{in}^{\infty} - \bar{\theta}_{sur}^{\infty}$ as a function of E

Fig. 3. Tunnel-air excess-temperature ($\bar{\theta}_{in}^{\infty}$) and the temperature difference between tunnel-air and tunnel-wall surface ($\bar{\theta}_{in}^{\infty} - \bar{\theta}_{sur}^{\infty}$) for $t \to \infty$ as a function of h, K_s, n, and E (time-averaged component).

3.1.4 Time-averaged heat flux through the tunnel-wall surface

To further understand the thermal processes in subway tunnels, the time-averaged heat flux through the tunnel-wall surface is calculated as follows.

Using Equations (6), (11), and (12), E can be expressed as

$$E = \rho_a q C_a (\bar{T}_{in}^{\infty} - \bar{T}_o) + \frac{1}{\frac{8R}{3K_s}+\frac{1}{h}} A\left(\bar{T}_{in}^{\infty} - T_g\right) \qquad (14)$$

Clearly, $\rho_a q C_a (\bar{T}_{in}^{\infty} - T_o)$ represents the time-averaged heat-flux, which is eliminated by ventilation. Let

$$\bar{E}_{sur} = \frac{1}{\frac{8R}{3K_s}+\frac{1}{h}} A\left(\bar{T}_{in}^{\infty} - T_g\right) \qquad (15)$$

with the unit W/m. $\bar{E}_{sur}$ represents the time-averaged heat-flux through the tunnel-wall surface per unit tunnel-length. In other words, $\eta_s = \bar{E}_{sur}/E$ defines the time-averaged heat-diffusion ratio through the surrounding soil. As shown in Fig. 4(a), η_s is very small for the standard case (η_s<2%), which means that, in general, ventilation is the most effective method to remove waste-heat from a subway tunnel. Thus, the heat recovery method (recommended by [49, 4]) from exhaust air through subway shafts could extract the majority of the waste heat generated in subway tunnels. Additionally, a higher h is not helpful to obtain a higher η_s if h>10 W/m^2·℃. This is because most of the thermal resistance occurs via heat conduction through the soil and not convective heat-transfer at the wall-surface like in the case h>10 W/m^2·℃. Fig. 4(b) reveals that η_s increases rapidly with increasing K_s, when K_s<30 W/m·℃. Furthermore, η_s increases to more than 50% when K_s increases to 30 W/m·℃. This confirms the finding that most thermal resistance occurs via heat conduction through the soil. However, if K_s is very high, the conductive thermal resistance may be as small as the

convective thermal resistance or even much smaller. In that case, a further increase in K_s can rarely increase η_s. If this is the case, the increase in h can increase η_s instead of K_s. This indicates that the influencing level of the influential factors of η_s could change as conditions change. Fig. 4(c) suggests that a higher n decreases η_s because more heat is eliminated via ventilation. Fig. 4(d) shows that a wider tunnel does not improve heat diffusion into the surrounding soil. In other words, a bigger R only increases the intensity of convective heat transfer but not the thermal conduction through the soil. As discussed above, increased convective heat-transfer does not increase the heat diffusion if most of the thermal resistance occurs through thermal conduction.

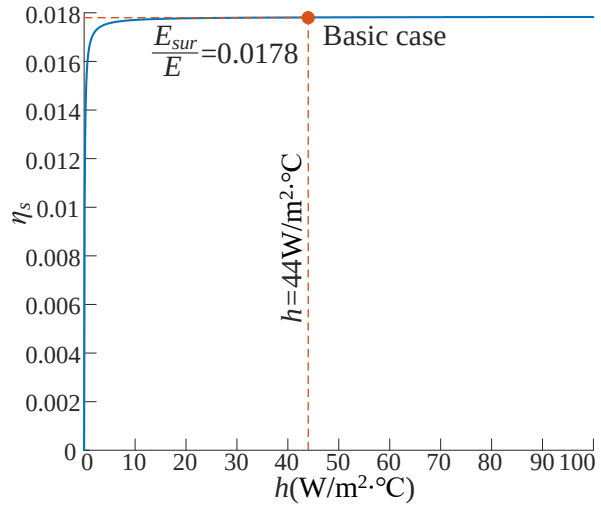

(a) η_s as a function of h

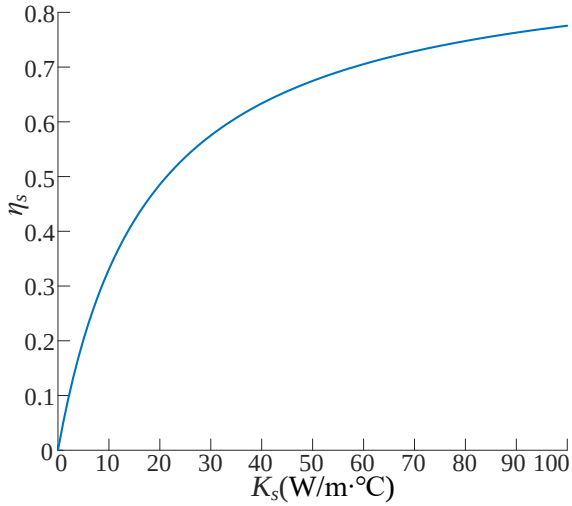

(b) η_s as a function of K_s

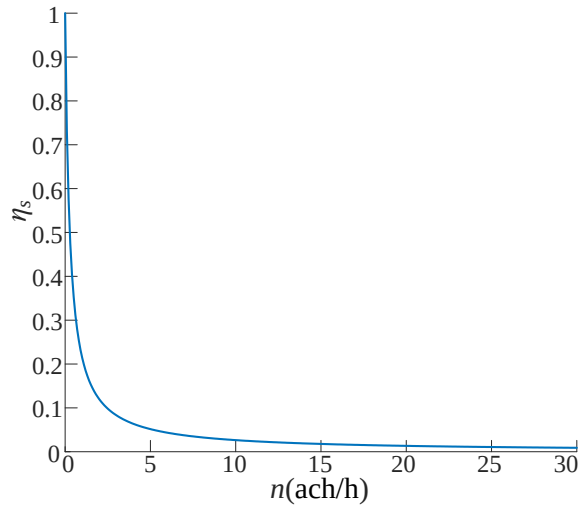

(c) η_s as a function of n

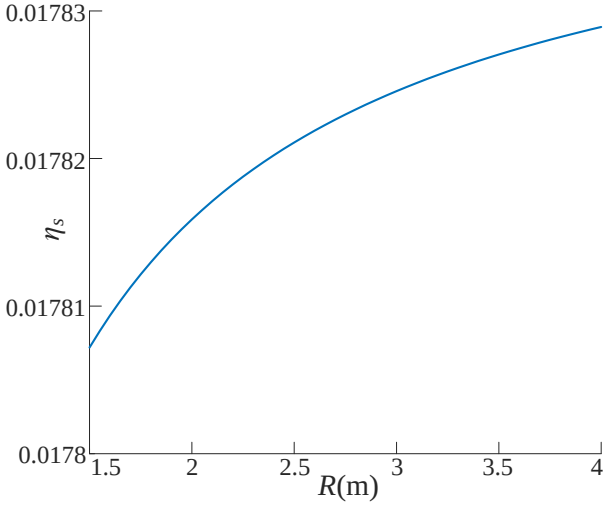

(d) η_s as a function of R

Fig. 4. Heat-diffusion ratio through surrounding soil (η_s) as a function of h, K_s, n, and R (time-averaged, $t \to \infty$).

3.2 Solution for the periodic components

3.2.1 Normalized-amplitude and phase shift of the tunnel-air temperature

The solution of the problem described by Equations (1) to (6) can be obtained by the separation of variables (see Appendix C):

$$\Delta\tilde{T}_{in} = f_{in/out}\Delta T_{out} cos(\omega t - \phi_{in-out}) \quad (16)$$

$$f_{in/out} = \frac{\Delta T_{in}}{\Delta T_{out}} = [(1+\lambda \mathrm{A}_1)^2 + (D+\lambda \mathrm{A}_2)^2]^{-0.5} \quad (17)$$

$$\phi_{in-out} = tan^{-1}\left(\frac{D+\lambda \mathrm{A}_2}{1+\lambda \mathrm{A}_1}\right) \quad (18)$$

where $A_1 = \dfrac{N_1^2\left(\frac{1}{\sqrt{Fo_{\mathrm{R}}^{\omega}}}\right)+Bi\sqrt{Fo_{\mathrm{R}}^{\omega}}N_0\left(\frac{1}{\sqrt{Fo_{\mathrm{R}}^{\omega}}}\right)N_1\left(\frac{1}{\sqrt{Fo_{\mathrm{R}}^{\omega}}}\right)\cos\left[\phi_1\left(\frac{1}{\sqrt{Fo_{\mathrm{R}}^{\omega}}}\right)+\frac{3}{4}\pi-\phi_0\left(\frac{1}{\sqrt{Fo_{\mathrm{R}}^{\omega}}}\right)\right]}{N_1^2\left(\frac{1}{\sqrt{Fo_{\mathrm{R}}^{\omega}}}\right)+Bi^2Fo_{\mathrm{R}}^{\omega}N_0^2\left(\frac{1}{\sqrt{Fo_{\mathrm{R}}^{\omega}}}\right)+2Bi\sqrt{Fo_{\mathrm{R}}^{\omega}}N_0\left(\frac{1}{\sqrt{Fo_{\mathrm{R}}^{\omega}}}\right)N_1\left(\frac{1}{\sqrt{Fo_{\mathrm{R}}^{\omega}}}\right)\cos\left[\phi_1\left(\frac{1}{\sqrt{Fo_{\mathrm{R}}^{\omega}}}\right)+\frac{3}{4}\pi-\phi_0\left(\frac{1}{\sqrt{Fo_{\mathrm{R}}^{\omega}}}\right)\right]}$,

$A_2 = \dfrac{Bi\sqrt{Fo_{\mathrm{R}}^{\omega}}N_0\left(\frac{1}{\sqrt{Fo_{\mathrm{R}}^{\omega}}}\right)N_1\left(\frac{1}{\sqrt{Fo_{\mathrm{R}}^{\omega}}}\right)\sin\left[\phi_1\left(\frac{1}{\sqrt{Fo_{\mathrm{R}}^{\omega}}}\right)+\frac{3}{4}\pi-\phi_0\left(\frac{1}{\sqrt{Fo_{\mathrm{R}}^{\omega}}}\right)\right]}{N_1^2\left(\frac{1}{\sqrt{Fo_{\mathrm{R}}^{\omega}}}\right)+Bi^2Fo_{\mathrm{R}}^{\omega}N_0^2\left(\frac{1}{\sqrt{Fo_{\mathrm{R}}^{\omega}}}\right)+2Bi\sqrt{Fo_{\mathrm{R}}^{\omega}}N_1\left(\frac{1}{\sqrt{Fo_{\mathrm{R}}^{\omega}}}\right)N_0\left(\frac{1}{\sqrt{Fo_{\mathrm{R}}^{\omega}}}\right)\cos\left[\phi_1\left(\frac{1}{\sqrt{Fo_{\mathrm{R}}^{\omega}}}\right)+\frac{3}{4}\pi-\phi_0\left(\frac{1}{\sqrt{Fo_{\mathrm{R}}^{\omega}}}\right)\right]}$,

$f_{in/out}$ is the attenuation ratio of the amplitude for the tunnel-air temperature compared to the outdoor temperature; ϕ_{in-out} is the phase shift of the tunnel-air temperature compared to the outdoor temperature, rad; $Fo_{\mathrm{R}}^{\omega} = \frac{a_s}{R^2\omega}$, $D = \frac{V}{q}\omega$. Fo_{R}^{ω} is the dimensionless time period. D is the ratio of the time scale for ventilation affecting the interior temperature to the time period [37].

The analytical solutions in Equations (16) to (18) are shown in Fig. 5 (daily period) and Fig. 6 (yearly period). Fig. 5 depicts $f_{in/out}$ and ϕ_{in-out} as functions of h, K_s, n, $\rho_s{\cdot}C_s$, and R for the daily period. It suggests that, for the daily period, $f_{in/out}$ varies significantly with h, K_s, n, $\rho_s{\cdot}C_s$, and R. This may be because the contribution of the five processes (internal heat

generation, ventilation, convective heat-transfer, heat conductivity and heat storage by effective thermal mass) are approximately of the same order of magnitude. In other words, a change in any process-contribution changes $f_{in/out}$. However, if the contribution of a process exceeds a certain magnitude, the corresponding effect would become weaker. This is illustrated by trend lines that become increasingly shallow - see Fig. 5(a) to (d). A similar trend could be found if *R* were large enough.

An interesting phenomenon is shown in Fig. 5(a): Here, $f_{in/out}$ is a non-monotonous function of *h*. This would be hard to explain with a physical principle. However, mathematically, this makes sense. On the other hand, $f_{in/out}$ changes monotonically with increasing K_s, *n*, $\rho_s \cdot C_s$, and *R*. Fig. 5(c) shows that $f_{in/out}$ increases as *n* increases. This is because the fluctuation of the tunnel-air temperature is caused by the fluctuation of the outdoor-air temperature. Hence, a larger *n* means a bigger driving force, and $f_{in/out}$ is higher. However, the increase in $f_{in/out}$ occurs more slowly for *n*>15 ach/h. This is because $f_{in/out}$ increases more slowly for a further increase in *n*, as the amplitude of the tunnel-air temperature approaches the amplitude of the outdoor-air temperature. Conversely, $f_{in/out}$ decreases as K_s, $\rho_s \cdot C_s$, and *R* increase. The increase in K_s, $\rho_s \cdot C_s$, and *R* can be interpreted as an increase in effective thermal mass. In other words, $f_{in/out}$ decreases monotonically with increasing effective thermal mass. This is consistent with the outcomes of a previous study [27]. Additionally, Fig. 5(b) suggests that $f_{in/out}$ drops from 0.94 to 0.48 when K_s increases from 0 to 10W/m·℃. However, the reduction slows down as K_s increases further. This is because, when K_s is high enough, the effective thermal mass is not the limiting factor for the thermal storage capacity any more. Instead, the thermal storage capacity may be limited by *h*, the temperature amplitude of the outdoor-air, or the period-length. In addition, Fig. 5(d) and (e) indicate that $f_{in/out}$ has a nearly linear relationship with $\rho_s \cdot C_s$ and *R*. It can also be

concluded that lining the tunnel with a phase-change material ($\rho_s \cdot C_s$ is larger), or digging a wider tunnel (R is larger), helps reduce $f_{in/out}$. The above methods that help to reduce $f_{in/out}$ would also help to decrease the peak temperature of the tunnel air, and thus help to mitigate overheating.

In addition, a higher h or wider R can increase the phase shift ϕ_{in-out}, while a larger n, decreases it. Knowing this can help engineers minimize any overlap of the tunnel-air temperature-peak with peak traffic hours in their tunnel structure designs. Interestingly, as shown in Fig. 5(b) and (d), ϕ_{in-out} is a non-monotonous function of K_s, and $\rho_s \cdot C_s$. This means that ϕ_{in-out} varies non-monotonously with the effective thermal mass. This finding is consistent with previously reported results [27].

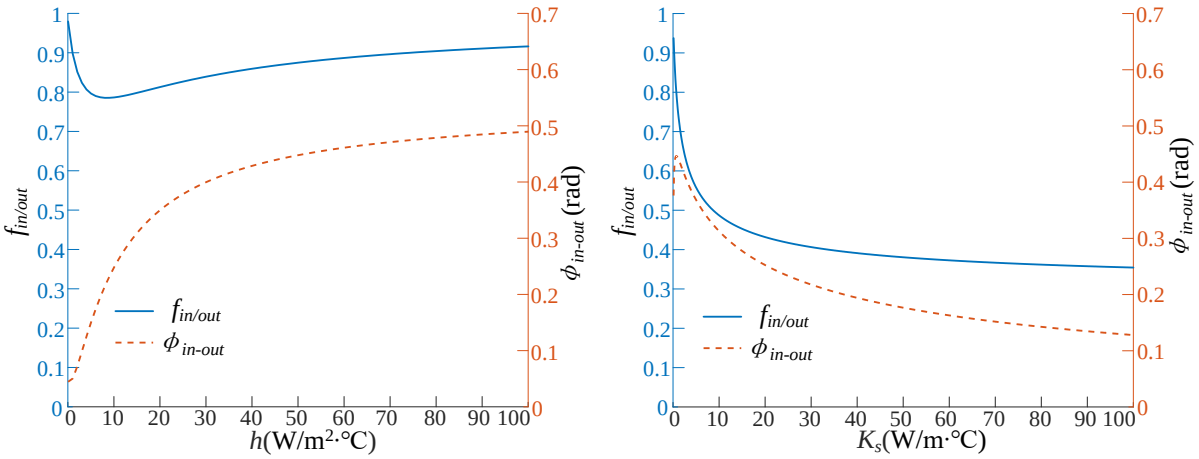

(a) $f_{in/out}$ and ϕ_{in-out} as a function of h (b) $f_{in/out}$ and ϕ_{in-out} as a function of K_s

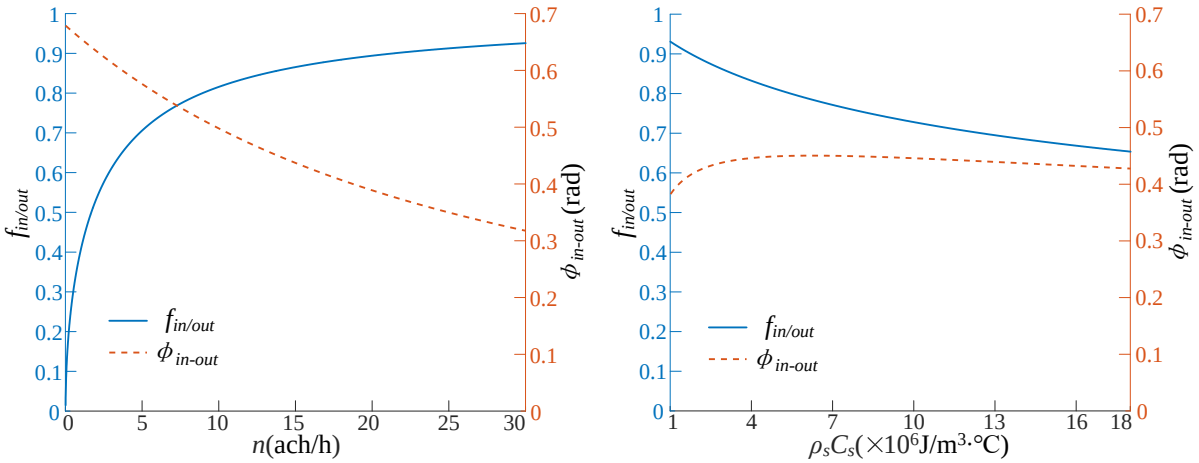

(c) $f_{in/out}$ and ϕ_{in-out} as a function of n (d) $f_{in/out}$ and ϕ_{in-out} as a function of $\rho_s \cdot C_s$

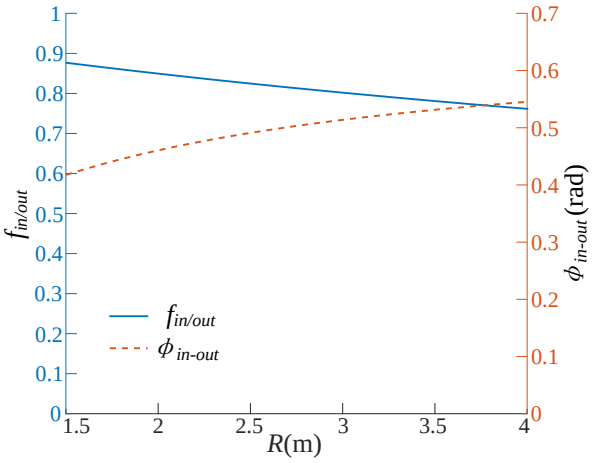

(e) $f_{in/out}$ and ϕ_{in-out} as a function of R

Fig. 5. Normalized-amplitude ($f_{in/out}$) and phase shift (ϕ_{in-out}) of the tunnel-air temperature as a function of h, K_s, n, $\rho_s \cdot C_s$, and R (daily period).

For the yearly period, Fig. 6 reveals that the amplitude of the tunnel-air temperature is rarely below the outdoor-air temperature (i.e. $f_{in/out} \rightarrow 1$) in most cases - see Fig 6(a), (c), (d), (e). Two exceptions are the conditions that n is extremely low or K_s is enhanced. The cause of the fluctuation of the tunnel-air temperature are out-door air-temperature changes. Thus, a very low n means that the driving force for the fluctuation is very small, i.e., $f_{in/out}$ is small. For K_s, according to Fig. 6(b), $f_{in/out}$ decreases as K_s increases. This means that $f_{in/out}$ decreases as the effective thermal mass increases. However, this effect is hardly noticeable in Fig. 6(d) and (e) because the range of $\rho_s \cdot C_s$ and R is too small to reveal any changes in $f_{in/out}$.

On the other hand, according to Fig. 6, the dependency of ϕ_{in-out} on the relevant parameters for the yearly period is similar to the daily period. An obvious difference is that ϕ_{in-out} shows a non-monotonic relation with $\rho_s \cdot C_s$ for the daily period but a monotonic relation for the yearly period, which is not straightforward to explain in terms of physics. In addition, the phase shift for the yearly period is generally below 0.2 (about 12 days) unless

n<5. However, this time-lag is not long enough to make the peak of tunnel-air temperature different from the peak of the outdoor temperature.

Additionally, by comparing Fig. 5 and Fig. 6, it is found that $f_{in/out}$ is generally smaller for the daily period than the yearly period. However, ϕ_{in-out} is larger. This could be because the damping effect of the thermal mass is smaller if the period is longer. The damping effect of the thermal mass would be stronger if the ratio of heat storage (by thermal mass) to the total internal heat generation during the period was larger. Clearly, the internal heat generation for the period increases linearly with increasing period-length. On the other hand, heat storage (by the thermal mass) increases slowly with increasing period-length. Consequently, there is a stronger damping effect for the daily period, i.e., smaller $f_{in/out}$ and larger ϕ_{in-out}. The same can also be concluded from the formulas published by Yam et. al. [27].

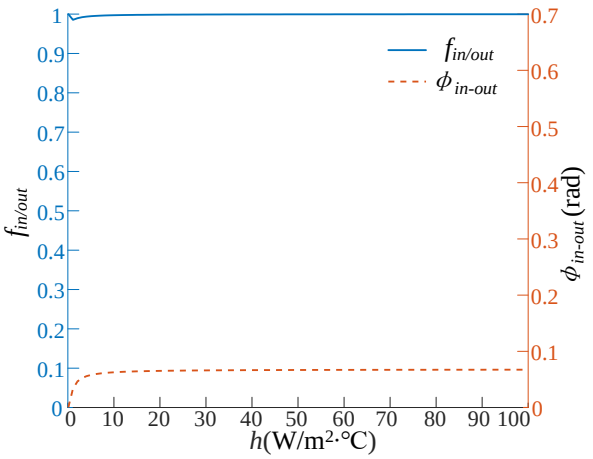

(a) $f_{in/out}$ and ϕ_{in-out} as a function of h

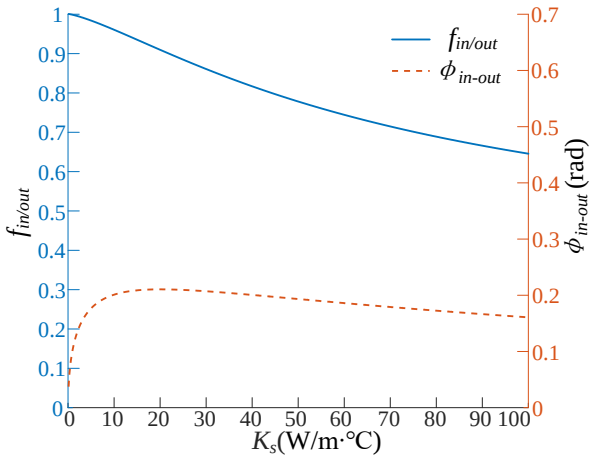

(b) $f_{in/out}$ and ϕ_{in-out} as a function of K_s

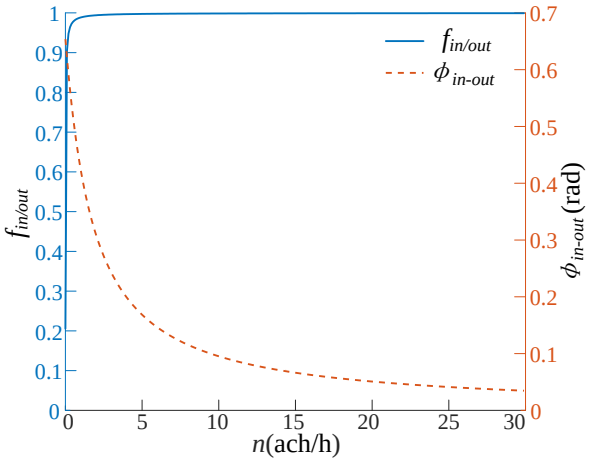

(c) $f_{in/out}$ and ϕ_{in-out} as a function of n

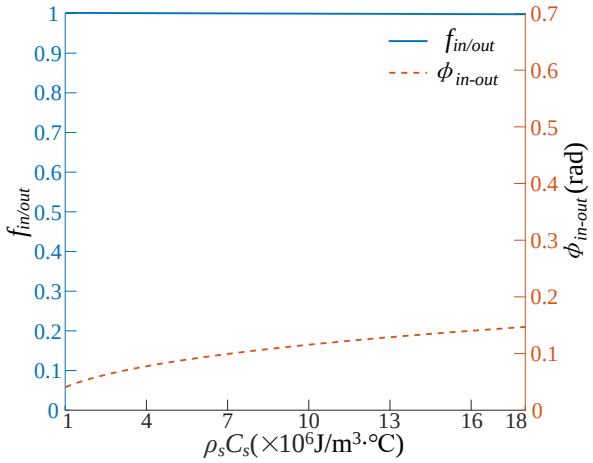

(d) $f_{in/out}$ and ϕ_{in-out} as a function of $\rho_s \cdot C_s$

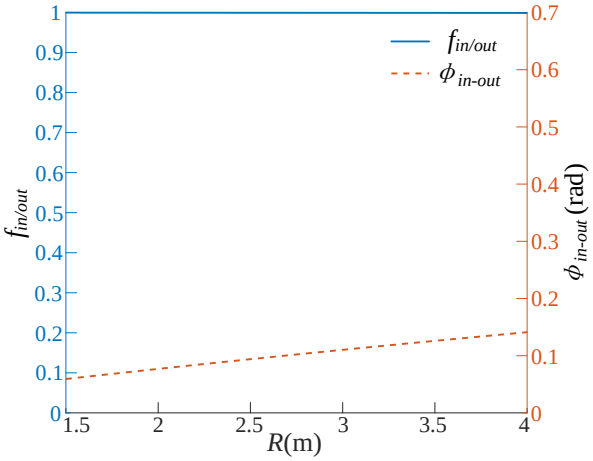

(e) $f_{in/out}$ and ϕ_{in-out} as a function of R

Fig. 6. Normalized-amplitude ($f_{in/out}$) and phase shift (ϕ_{in-out}) of the tunnel-air temperature as a function of h, K_s, n, $\rho_s \cdot C_s$, and R (yearly period).

3.2.2 Normalized-amplitude and phase shift of the surrounding-soil temperature

The relationship between the periodic components of the tunnel-air temperature and the soil temperature can be obtained by eliminating the dimensions for the results of Reference [35]:

$$\Delta\tilde{T}_s = f_{s/in} f_{in/out} \Delta T_{out} cos(\omega t - \phi_{in-out} - \phi_{s-in}) \quad (19)$$

$$f_{s/in} = \frac{\Delta T_s}{\Delta T_{in}} = \frac{N_0\left(\frac{z}{\sqrt{Fo_R^{\omega}}}\right)}{\sqrt{\alpha^2+\beta^2}} \quad (20)$$

$$\phi_{s-in} = \phi_0\left(\frac{z}{\sqrt{Fo_R^{\omega}}}\right) - tan^{-1}\left(\frac{\beta}{\alpha}\right) \quad (21)$$

Here, $z = \frac{r}{R}$,

$$\alpha = N_0\left(\frac{1}{\sqrt{Fo_R^{\omega}}}\right)\cos\left[\phi_0\left(\frac{1}{\sqrt{Fo_R^{\omega}}}\right) + \frac{1}{Bi\sqrt{2Fo_R^{\omega}}}N_1\left(\frac{1}{\sqrt{Fo_R^{\omega}}}\right)\left\{\cos\left[\phi_1\left(\frac{1}{\sqrt{Fo_R^{\omega}}}\right) + \frac{1}{2}\pi\right] - \sin\left[\phi_1\left(\frac{1}{\sqrt{Fo_R^{\omega}}}\right) + \frac{1}{2}\pi\right]\right\}\right],$$

$$\beta = N_0\left(\frac{1}{\sqrt{Fo_R^{\omega}}}\right)\sin\left[\phi_0\left(\frac{1}{\sqrt{Fo_R^{\omega}}}\right)\right] + \frac{1}{Bi\sqrt{2Fo_R^{\omega}}}N_1\left(\frac{1}{\sqrt{Fo_R^{\omega}}}\right)\left\{\cos\left[\phi_1\left(\frac{1}{\sqrt{Fo_R^{\omega}}}\right) + \frac{1}{2}\pi\right] + \sin\left[\phi_1\left(\frac{1}{\sqrt{Fo_R^{\omega}}}\right) + \frac{1}{2}\pi\right]\right\},$$

$f_{s/in}$ is the attenuation ratio of the amplitude of the soil temperature to the tunnel-air temperature; ϕ_{s-in} is the phase shift of the soil temperature compared to the tunnel-air temperature, rad. Similarly, $f_{s/sur}$ is defined as the attenuation ratio of the amplitude of the soil temperature to the tunnel-wall surface temperature; and ϕ_{s-sur} is the phase shift of the soil temperature with respect to the tunnel-wall surface temperature, rad. Based on Equations (19) to (21), Fig. 7 illustrates how $f_{s/sur}$ and ϕ_{s-sur} change as r and a_s changes for the yearly period. This suggests that $f_{s/sur}$ decreases quasi-linearly with increasing ln(r/R) first, and then much slower after $f_{s/sur}\approx 0.1$. In other words, the amplitude of the soil-temperature changes sharply near the tunnel-wall surface and less in the remote area. As shown in Fig. 7(b), however, ϕ_{s-sur} increases linearly with increasing r/R. In addition, $f_{s/sur}$ increases with increasing a_s, while, for ϕ_{s-sur}, the opposite happens. This is because the soil temperature tends to follow the temperature of the tunnel-wall surface closer when a_s is higher. Formulas (19) to (21) and Fig. 7 show a good way to predict the soil-temperature fluctuation surrounding subway tunnels. This is very important to be able to estimate thermal stress in underground constructions. Similarly, it is easy to obtain the results for the daily period, which is omitted here.

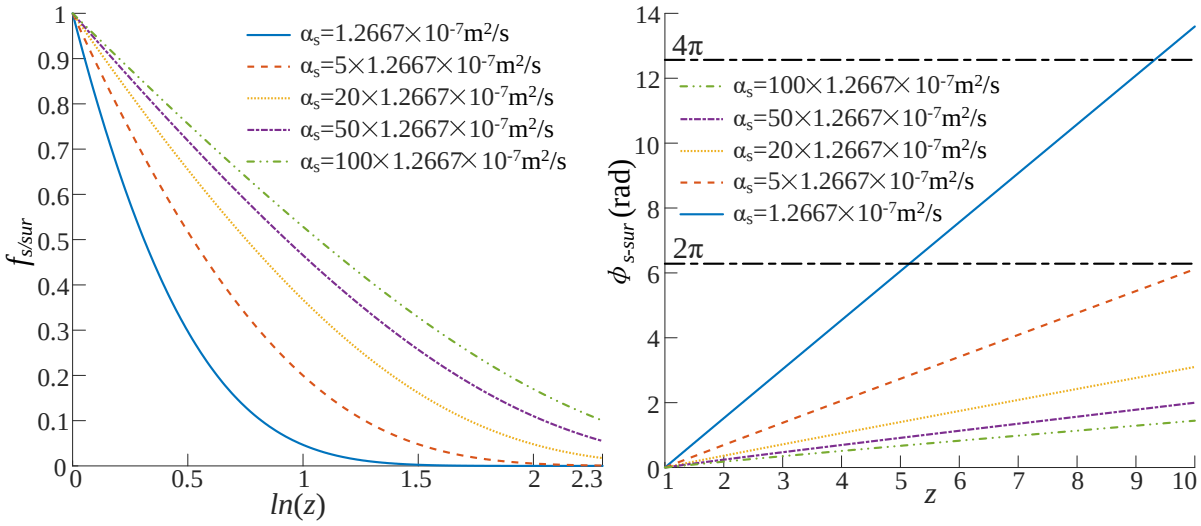

(a) $f_{s/sur}$ as a function of z and α_s (b) ϕ_{s-sur} as a function of z and α_s

Fig. 7. Normalized-amplitude ($f_{s/sur}$) and phase shift (ϕ_{s-sur}) of the soil temperature as a function of z and α_s (periodic component, yearly period).

3.2.3 Amplitude of the heat flux at the surface of the tunnel-wall

Using Equations (16) to (18), the periodic component of the heat flux through the tunnel-wall surface $\Delta\tilde{E}_{sur}$ is:

$$\Delta\tilde{E}_{sur} = \Delta E_{sur} cos(\omega t - \phi_{in-out} - \phi_{E-in}) \quad (22)$$

$$\Delta E_{sur} = 2\pi R h f_{in/out} \Delta T_{out} \sqrt{1 + f_{s/in}^2 - 2 f_{s/in} cos(\phi_{s-in})} \quad (z = 1) \quad (23)$$

$$\phi_{E-in} = tan^{-1} \frac{f_{s/in} sin(\phi_{s-in})}{1 - f_{s/in} cos(\phi_{s-in})} \quad (z = 1) \quad (24)$$

Here, ΔE_{sur} is the amplitude of the heat flux through the tunnel-wall surface per unit tunnel-length, W/m; ϕ_{E-in} is the phase shift of the heat flux with respect to the tunnel-air temperature, rad. Setting $\Delta\eta_s = \Delta E_{sur}/E$ represents the dimensionless heat-flux amplitude through the tunnel-wall surface, normalized by the internal heat source E.

Fig. 8 shows how $\Delta\eta_s$ and ϕ_{E-in} change as a function of h, K_s, n, $\rho_s \cdot C_s$, and R for the yearly period. As shown, $\Delta\eta_s$ shows similar trends for a changing h and n- see Fig. 8 (a) and (c). For h and $\Delta\eta_s$ not much changes when h>10 W/ m$^{2\cdot}$℃. This is because the heat-storage

capacity of the surrounding soil is limited mostly by the conduction process rather than the convective heat transfer process here. As a result, an even higher h could contribute little to increase thermal storage. A changing n causes a similar trend as h. This is because the thermal energy, which is transported by ventilation air, can not fully transfer to the soil if n is very high (soil is a poor heat-conductor). Conversely, $\Delta\eta_s$ changes with K_s, $\rho_s \cdot C_s$, and R not so abruptly. Clearly, $\Delta\eta_s$ increases with increasing K_s, $\rho_s \cdot C_s$, and R. In other words, $\Delta\eta_s$ increases with increasing effective thermal mass. Similarly, the results for the daily period can be obtained easily, which are omitted here.

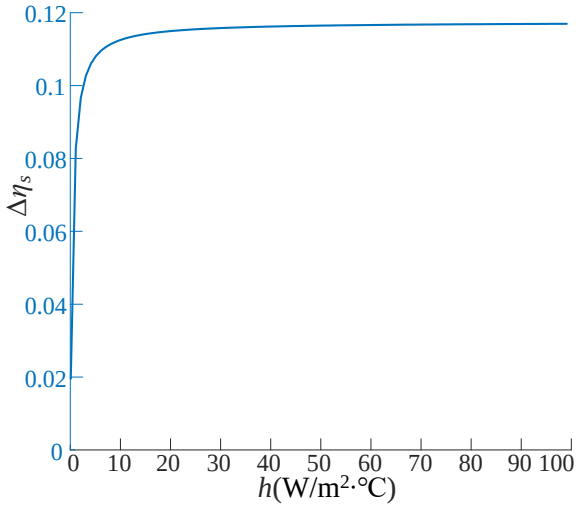

(a) $\Delta\eta_s$ as a function of h

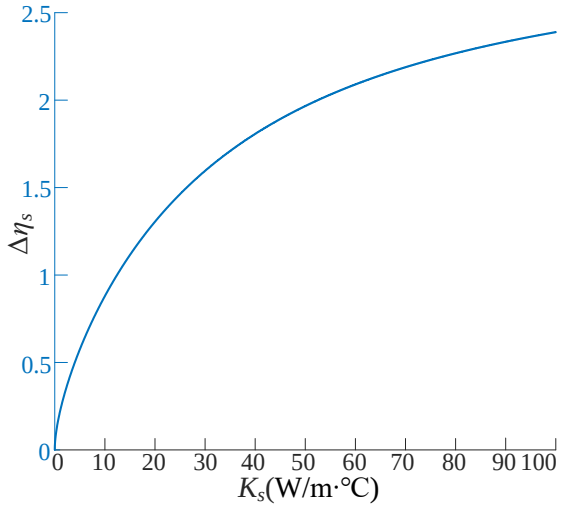

(b) $\Delta\eta_s$ as a function of K_s

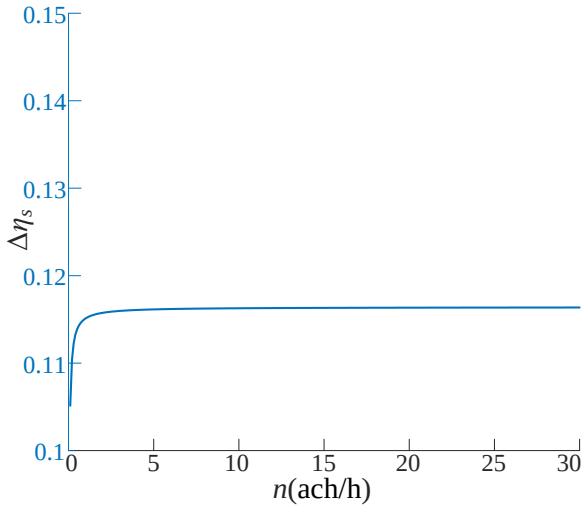

(c) $\Delta\eta_s$ as a function of n

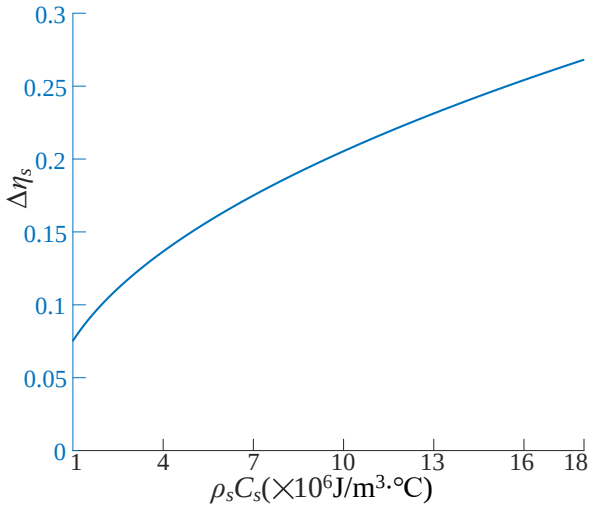

(d) $\Delta\eta_s$ as a function of $\rho_s \cdot C_s$

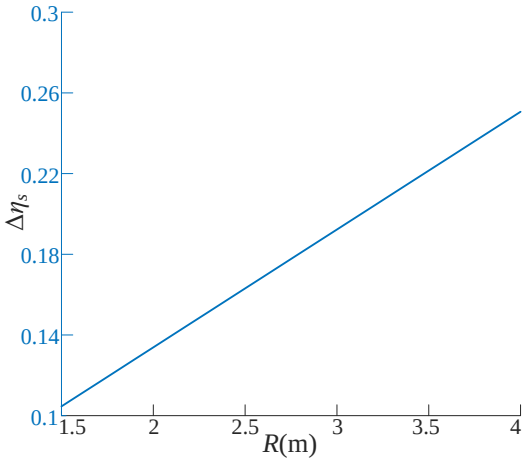

(e) $\Delta\eta_s$ as a function of R

Fig. 8. Normalized-amplitude of the heat-flux through the tunnel-wall surface ($\Delta\eta_s$) as a function of h, K_s, n, $\rho_s \cdot C_s$, and R (yearly period).

4 Validation and application of the model in London Underground

4.1 Validation of the model in London Underground

To validate the above model, a comparison between the measured value and the calculated results was conducted. The month-averaged tunnel-air temperature in the Sub-surface-lines of London Underground was considered. The measured values in 2017 [7] and the predicted trend generated from the model are shown in Fig. 9. The predicted results generally agree well with the measurement. Small discrepancy occurs from July to October. This is likely due to the employment of sinusoidal form in the mathematical model, while the actual ambient temperature in a specific year may not follow the exact sinusoidal trend.

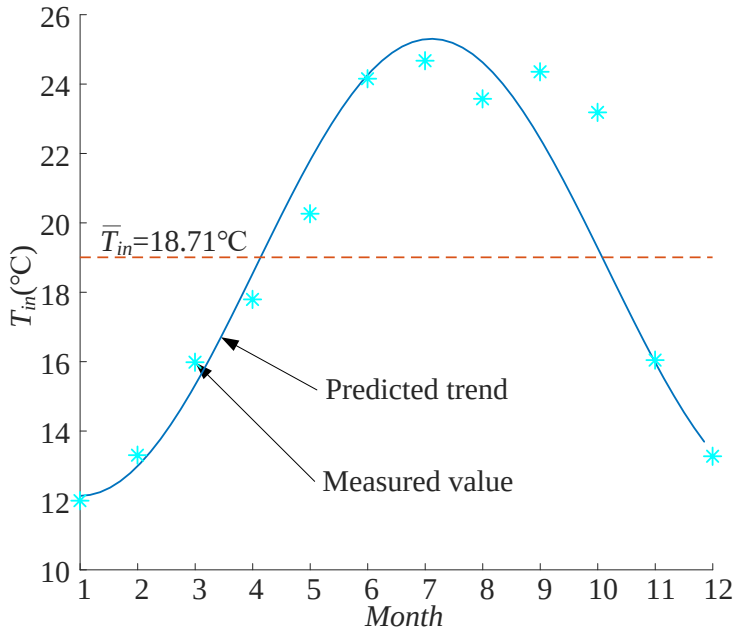

Fig. 9. A comparison between measured values and calculated trend of tunnel-air temperature in the Sub-surface Line of London Underground.

4.2 Application of the model in London Underground

The above model could be used (but not limited) to analyse how overheating in subway tunnels (e.g., London Underground) is affected by global warming ($\bar{T}_{\mathrm{out}}$) and increasing internal heat-source (E) caused by increasing passengers. Fig. 10 shows how the maximum tunnel-air temperature T_{in}^{max} and overheating degree-hours (T_{in} >28℃) increase with increasing internal heat source E and annual-averaged ambient temperature $\bar{T}_{\mathrm{out}}$. In the calculation of T_{in}^{max} and overheating degree-hours, all properties were based on the conditions in a London underground (i.e. n=15 ach/h, h=44 W/m^2·℃, K_s=0.35 W/m·℃, ρ_s =1500 kg/m^3, C_s =1842 J/kg·℃, R=1.7m) [35]. Based on the weather condition of London [50], daily average temperature of tunnel air was calculated by assuming the amplitude of 5 ℃ for the ambient temperature in yearly-period. Then hourly average temperature of tunnel air was calculated by assuming the amplitude of 5℃ for the ambient temperature in daily-period. As shown in Fig. 10-a, T_{in}^{max} has a positive linear relationship with $\bar{T}_{\mathrm{out}}$ and E. T_{in}^{max}

could be higher than 40℃ if $\bar{T}_{\text{out}}$ is increased to 20℃ and E to 500W/m. Overheating degree-hours shows a curved surface in the $\bar{T}_{\text{out}}$-E plane (Fig. 10-b). When $\bar{T}_{out}$ is small, the impact of E on overheating is limited. When $\bar{T}_{\text{out}}$ and E become higher, their joint impact on overheating degree-hours is much stronger. The combined influence of $\bar{T}_{out}$ and E could explain the aggravated overheating risk in London Underground recently.

Note that ideal models of T_{out} (cosine wave) and E (constant) are used in this study. That means the climate extreme (e.g., heatwave) and diurnal change of E (e.g., high E during peak traffic hours) are not considered in this model. However, this is still a general applicable explanation on how T_{in}^{max} and overheating degree-hours could change with global warming and increasing internal heat-source. Additionally, the change in $\bar{T}_{\text{out}}$ also could be considered as a change in geographical location instead of global warming and could be applied in different cities in different climates.

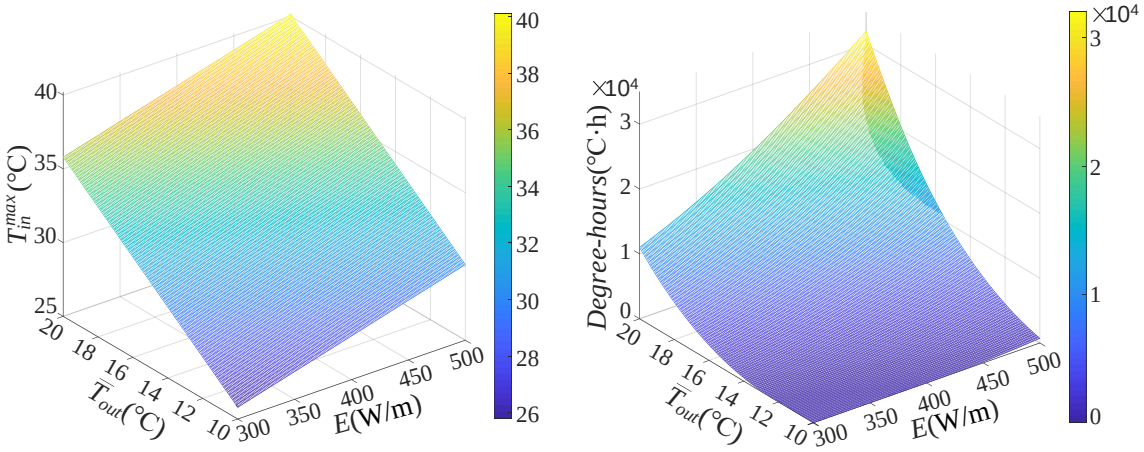

(a) T_{in}^{max} as a function of E and $\bar{T}_{\text{out}}$ (b) Overheating Degree-hours as a function of E and $\bar{T}_{\text{out}}$

Fig. 10. The maximum tunnel-air temperature (T_{in}^{max}) and Overheating Degree-hours (T_{in} >28℃) as a function of internal heat-source (E) and annual-averaged ambient temperature ($\bar{T}_{\text{out}}$).

5 Discussion

5.1 Methods to control tunnel-air temperature

Only the methods to reduce tunnel-air temperature in summer are discussed here in detail. The methods to increase the tunnel-air temperature in winter can be obtained in a similarly way.

Considering the solutions for both the time-averaged and the periodic components, there are seven parameters that affect the tunnel-air temperature - see Table 1. However, ρ_s and C_s can be treated as one parameter because they always appear together as the product of $\rho_s \cdot C_s$. Among these parameters, E affects the time-averaged component only, while $\rho_s \cdot C_s$ affects the periodic component only. The methods to reduce the tunnel-air temperature in summer are estimated using a five-star ranking. This is done by taking both the time-averaged and periodic components into account, and by considering both daily period and yearly period without a logical derivation process.

As shown in Table 1, mechanical ventilation via a suitable air change rate n is the priority option because it is highly effective and inexpensive. However, the effectiveness is limited when n is very high. The second-best solution to reduce tunnel-air temperature is to reduce E. A regenerative braking-system and deliberately slanted tunnels are helpful to reduce E. The third-best solution is to raise K_s by adding thermal-tube. However, many thermal tubes may be needed, and the workload of the thermal-tube installation is heavy. Additionally, this plan is difficult to be applied to reconstruction projects. In the range of practice interest, the increases in R, $\rho_s \cdot C_s$, and h have slight effect on tunnel-air temperature. Thus, the plans of changing R, $\rho_s \cdot C_s$, and h to reduce tunnel-air temperature are not recommended. If the tunnel-air temperature could not be cooled down properly by the above methods, an active cooling or heat-recovery system may be needed. This approach could become a necessity soon, due to both increasing internal heat-source in subway tunnels and global warming. The disadvantage of this plan is that additional equipment are required. Also, the security in subway tunnels could be threatened by leaking water or refrigerant from the active cooling system.

555 The results shown in Table 1 are based on the assumption that only one parameter changes
556 similar to the standard scenario. If more than one parameter changes, the corresponding
557 impact should be analyzed using the solutions presented above.

Table 1 Summary of known methods used to control tunnel-air temperature.

Parameter	Time-averaged Component	Periodic Component		Action	Method	Difficulty/Disadvantage	Five-star ranking
		Year	Day				
n	Correlation: negative Trend: sharp to flat	Correlation: positive Trend: sharp to flat	Correlation: positive Trend: sharp to flat	The increase in n helps reduce the time-averaged temperature but hinders the reduction of the temperature amplitude.	Mechanical ventilation	1. While it is advantageous to enhance ventilation, a too high n decreases efficiency.	★★★★
E	Correlation: positive Trend: linear	——	——	If E decreases, both the time-averaged and the peak temperature can be lowered. The reduction of the time-averaged temperature helps reduce the energy consumption of air-conditioning in trains and stations.	1.Using a regenerative braking-system 2. Deliberately slanted tunnel 3. Applying an active cooling system or heat recovery system	1. The method relies on technological advancement to increase the efficiency of the machinery and regenerative braking system. 2. A large quantity of equipment and tubes are needed to actively cool or recover heat from the tunnel. 3. Large amount of earthwork needed to produce a suitable slant.	★★★
K_s	Correlation: negative Trend: sharp to flat	Correlation: negative Trend: quasi-linear	Correlation: negative Trend: sharp to flat	The increase in K_s can reduce both the average value and the amplitude of the tunnel-air temperature. Thus, it is helpful to reduce both average and peak temperature.	Adding thermal tubes	1. Many thermal tubes may be needed. The workload of the thermal-tube installation is heavy. It is difficult to be applied to reconstruction projects. 2. It requires further study to determine how deep the thermal tubes should extent.	★★
R	——	——	Correlation: positive Trend: linear	The increase in R can slightly reduce the temperature amplitude for the daily period.	Widening of the tunnel	1. A large volume of extra earthwork and underground space is needed. 2. Only the peak temperature is reduced slightly but not the average temperature.	★
$\rho_s \cdot C_s$	——	——	Correlation: negative Trend: sharp to flat	The increase in $\rho_s \cdot C_s$ can reduce the temperature amplitude for the daily period.	Adding phase change material	1. A large volume of extra earthwork and phase change material is needed. 2. Only the peak temperature is reduced slightly but not the average temperature.	★
h	——	——	Correlation: negative/positive Trend: non-monotonous	A suitable h can produce the minimum amplitude for the tunnel-air temperature for the daily period.	Choosing the right material, surface roughness, or adding wings.	1. The temperature amplitude is only slightly reduced. 2. The target range for h is too narrow, which makes it hard to maintain within a suitable range.	☆

5.2 Methods to achieve a suitable time-leg

We are more interested in the time-leg for the daily period than the yearly period because there is a certain risk that the tunnel-air temperature peak coincides with peak traffic hours, which are 4:00 pm to 6:00pm in London (5:00pm to 8:00pm in Beijing). The peak of the ambient temperature occurs at about 2:00pm. As shown in Fig. 5, for the standard scenario, the time leg is 1.7 h - a phase shift of 0.44. In addition, the largest time leg for the considered scenarios is 2.6h - and the phase shift is 0.67, see Fig. 5(c). This indicates that it is impossible to delay the tunnel-air temperature peak long enough to occur only after peak traffic. Thus, a smaller time-leg should be more helpful to keep the tunnel-air temperature-peak away from the traffic-peak. Unfortunately, a higher h and R generally causes a larger time-leg, while the increase in $\rho_s \cdot C_s$ affects the phase shift very little. However, increasing K_s to exceed 10 W/m·℃ can visibly reduce the time leg. This shows another benefit of adding thermal tubes near subway tunnels.

5.3 Limitations and applications

While this study introduced a more detailed model for subway tunnels and found analytical solutions with rigorous derivation, it should be noted that there are, of course, certain limitations. The ideal physical model uses a series of assumptions: a constant ventilation flow rate, a constant internal heat source, thoroughly mixed tunnel-air, and a negligible effect of underground water among others. Despite these limitations, the study offers a clear understanding how different thermal processes function together in subway tunnels and a logical method to identify and assess influential factors of tunnel temperatures. These findings provide an essential basis for the exploration of methods to reduce overheating in subway tunnels. The described methods to reduce the air temperature in the tunnel in summer can be used to improve both subway-tunnel design and operation. In a similar way, using the

described solutions, it is also possible to seek solutions to increase a tunnel's air temperature in winter.

6 Conclusion

An analytical model to predict the in-tunnel air temperature was developed that can describe the thermal processes in deeply buried subway tunnels. The following conclusions can be drawn:

i) The time-averaged component of tunnel-air temperature will approach steady state as the time tends to infinity, which has a positive linear relation with internal heat-source and average ambient temperature. Compared with outdoor air, the amplitude of the tunnel-air temperature shows a significant reduction in the day period but not in the year period.

ii) The time-averaged surrounding soil temperature will keep changing for thousands of years. In the long-term, more than 98% of the waste heat generated in the subway tunnels could be removed via ventilation.

iii) Based on the analytical solutions, a five-star ranking of the mitigation methods to reduce the tunnel-air temperature was applied. Mechanical ventilation with a suitable air-change rate was the best-ranked method. The second best method was to reduce internal heat generation. Active cooling or heat-recovery systems could soon become a necessity in subway tunnels due to both global warming and increasing inner heat-source.

Acknowledgements

This research was supported by the National Natural Science Foundation of China (No. 51408457), and the State Scholarship Fund awarded by the China Scholarship Council (No. 201807835013).

Appendix A

Substituting $\bar{\theta}_s = \bar{T}_s - T_g$, $\bar{\theta}_{in} = \bar{T}_{in} - T_g$, $\bar{\theta}_{sur} = \bar{T}_{sur} - T_g$, and $\theta_b = \bar{T}_{out} + \frac{E}{\rho_a q C_a} - T_g$ to (1) to (7), and applying the Laplace transform to (1), (2), and (6), we can write:

$$\frac{d^2\Theta_s}{dr^2} + \frac{1}{r}\frac{d\Theta_s}{dr} - \frac{p}{a_s}\Theta_s = 0 \qquad \text{(A1)}$$

$$-R\,\frac{d\Theta_s}{dr}|_{sur} = Bi(\Theta_{in} - \Theta_{sur}) \qquad \text{(A2)}$$

$$\frac{\theta_b}{p} - \Theta_{in} - \lambda(\Theta_{in} - \Theta_{sur}) = \frac{V}{q}p\Theta_{in} \qquad \text{(A3)}$$

Let $\zeta = \sqrt{p/a_s}$, then the solution for (A1) is:

$$\Theta_s = C_1 I_0(\zeta r) + C_2 K_0(\zeta r) \qquad \text{(A4)}$$

Here, I_0 and K_0 are the modified Bessel functions of the first and second kind, with the integer 0. Considering (3), $C_1 = 0$. Thus,

$$\Theta_s = C_2 K_0(\zeta r) \qquad \text{(A5)}$$

Since $\frac{\mathrm{dK_0(\zeta r)}}{\mathrm{dr}} = -\zeta \mathrm{K_1(\zeta r)}$, using Equations (2) and (A3) we can formulate:

$$\zeta R C_2 K_1(\zeta R) = Bi\big(\Theta_{in} - C_2 K_0(\zeta R)\big) \qquad \text{(A6)}$$

$$\frac{\theta_b}{p} - \Theta_{in} - \lambda\big(\Theta_{in} - C_2 K_0(\zeta R)\big) = \frac{V}{q}p\Theta_{in} \qquad \text{(A7)}$$

Here, K_1 is the modified Bessel function of the second kind with the integer 1. From Equations (A5) to (A7) θ_{in} and θ_s can be expressed as:

$$\Theta_{in} = \frac{\theta_b}{p} \cdot \frac{\zeta R K_1(\zeta R) + Bi K_0(\zeta R)}{Bi\left(1+\frac{V}{q}p\right)K_0(\zeta R) + \zeta R\left(1+\lambda+\frac{V}{q}p\right)K_1(\zeta R)} \qquad \text{(A8)}$$

$$\Theta_s = \frac{\theta_b}{p} \cdot \frac{Bi K_0(\zeta r)}{Bi\left(1+\frac{V}{q}p\right)K_0(\zeta R) + \zeta R\left(1+\lambda+\frac{V}{q}p\right)K_1(\zeta R)} \qquad \text{(A9)}$$

After applying the inverse Laplace transform to Equation (A8), $\bar{\theta}_{in}$ can be expressed as:

$$\bar{\theta}_{in} = \frac{\theta_b}{2\pi i}\int_{\delta-i\infty}^{\delta+i\infty} \frac{e^{pt}}{p} \cdot \frac{\zeta R K_1(\zeta R) + Bi K_0(\zeta R)}{Bi\left(1+\frac{V}{q}p\right)K_0(\zeta R) + \zeta R\left(1+\lambda+\frac{V}{q}p\right)K_1(\zeta R)}\, dp = \frac{\theta_b}{2\pi i}\int_{\delta-i\infty}^{\delta+i\infty} \frac{e^{pt}}{p} f(\zeta)\, dp \quad \text{(A10)}$$

Applying the contour integral method, $\bar{\theta}_{in}$ can be expressed as:

$$\bar{\theta}_{in} = \frac{2\theta_b}{\pi}\int_0^{\infty} \frac{e^{-(uR)^2 Fo} - 1}{u} g(uR) du \quad \text{(A11)},$$

where $g(uR) = \frac{g_2(uR)\left[\frac{uR}{Bi}J_1(uR) + J_0(uR)\right] - g_1(uR)\left[\frac{uR}{Bi}Y_1(uR) + Y_0(uR)\right]}{{g_1}^2(uR) + {g_2}^2(uR)}$,

$$g_1(uR) = \frac{uR}{Bi}\left[1 + \lambda - \left(\frac{R^2}{a_s}\right)^{-1}\frac{V}{q}(uR)^2\right]J_1(uR) + \left[1 - \left(\frac{R^2}{a_s}\right)^{-1}\frac{V}{q}(uR)^2\right]J_0(uR),$$

$$g_2(uR) = \frac{uR}{Bi}\left[1 + \lambda - \left(\frac{R^2}{a_s}\right)^{-1}\frac{V}{q}(uR)^2\right]Y_1(uR) + \left[1 - \left(\frac{R^2}{a_s}\right)^{-1}\frac{V}{q}(uR)^2\right]Y_0(uR).$$

Through similar methods and processes, $\bar{\theta}_s$ can be expressed as:

$$\bar{\theta}_s = \frac{2\theta_b}{\pi}\int_0^{\infty}\frac{e^{-(uR)^2Fo}-1}{u}j(uR,ur)du \quad \text{(A12)},$$

where $j(uR,ur) = \frac{g_2(uR)J_0(ur)-g_1(uR)Y_0(ur)}{{g_1}^2(uR)+{g_2}^2(uR)}$.

Clearly,

$$\bar{\theta}_{sur} = \frac{2\theta_b}{\pi}\int_0^{\infty}\frac{e^{-(uR)^2Fo}-1}{u}j(uR,uR)du \quad \text{(A13)}$$

Appendix B

Note that, after a sufficient long time, the term $\frac{d\bar{T}_{in}}{dt}$ in Equation (6) can be ignored for the calculation of the soil temperature [27]. Hence, after applying the Laplace transform to Equation (1) and considering the boundary condition Equation (2), Θ_{sur} can be expressed as:

$$\Theta_{sur} = \frac{1}{p}\cdot\frac{BiK_0(\zeta r)}{BiK_0(\zeta R)+\zeta R(1+\lambda)K_1(\zeta R)}(\bar{T}_0 + T_E - T_g) \qquad \text{(B1)},$$

where $\zeta = \sqrt{\frac{p}{a_s}}$. Substituting the Bessel function approximating expression $K_0(x) = \sqrt{\frac{\pi}{2x}}e^{-x}$ and $K_1(x) = \sqrt{\frac{\pi}{2x}}e^{-x}\left(1 + \frac{3}{8x}\right)$ into (B1), Θ_{sur} can be expressed as:

$$\Theta_{sur} = \frac{\theta_b}{p}\cdot\frac{1}{\zeta+\Omega} \qquad \text{(B2)}$$

Applying the inverse Laplace transform, the expression of $\bar{\theta}_{sur}$ is:

$$\bar{\theta}_{sur} = \frac{\theta_b}{1+\frac{3}{8Bi}(1+\lambda)}\left[1 - e^{\Omega^2 a_s t}erfc\left(\Omega\sqrt{a_s t}\right)\right] \quad \text{(B3)},$$

where

$$\Omega = \frac{3}{8R} + \frac{Bi}{R(1+\lambda)},$$

Considering $t \to +\infty$, according to the L'Hospital's rule, we can formulate:

$$\bar{\theta}_{sur}^{\infty} = \frac{8Bi\theta_b}{8Bi+3\lambda+3} \qquad \text{(B4)}$$

Since $\lim_{t\to+\infty} \frac{d\bar{\theta}_{in}}{dt} = 0$, substituting Equation (B4) into Equation (A3), $\bar{\theta}_{in}^{\infty}$ can be expressed as:

$$\bar{\theta}_{in}^{\infty} = \frac{(8Bi+3)\theta_b}{8Bi+3\lambda+3} \qquad \text{(B5)}$$

Appendix C

Let $\Delta\tilde{T}_{out} = \Delta T_{out}e^{i\omega t}$, $\Delta\tilde{T}_{in} = \Delta T_{in}e^{i\omega t}$, $\Delta\tilde{T}_s = \Delta T_s e^{i\omega t}$, $\Delta\tilde{T}_{sur} = \Delta T_{sur}e^{i\omega t}$ [35], and substituting them into Equations (22), (23), and (27), we get:

$$\Delta\tilde{T}_{out} - \Delta\tilde{T}_{in} - \lambda\left(\Delta\tilde{T}_{in} - \Delta\tilde{T}_{sur}\right) = iD\Delta\tilde{T}_{in} \qquad \text{(C1)}$$

$$\frac{d^2\Delta\tilde{T}_s}{dr^2} + \frac{d\Delta\tilde{T}_s}{rdr} - \frac{i\omega}{a_s}\Delta\tilde{T}_s = 0 \qquad \text{(C2)}$$

$$-R\frac{d\Delta\tilde{T}_s}{dr}|_{sur} = Bi\left(\Delta\tilde{T}_{in} - \Delta\tilde{T}_{sur}\right) \qquad \text{(C3)}$$

The solution to Equation (C2) is

$$\Delta\tilde{T}_s = C_3 I_0\left(\sqrt{\frac{i\omega}{a_s}}r\right) + C_4 K_0\left(\sqrt{\frac{i\omega}{a_s}}r\right) \qquad \text{(C4)}$$

Considering Equation (24), $C_3 = 0$. Thus,

$$\Delta\tilde{T}_s = C_4 K_0\left(\sqrt{\frac{i\omega}{a_s}}r\right) \qquad \text{(C5)}$$

From Equations (C3) and (C5), $\Delta\tilde{T}_{sur}$ can be expressed as:

$$\Delta\tilde{T}_{sur} = \frac{Bi\Delta\tilde{T}_{in}K_0\left(\sqrt{\frac{i\omega}{a_s}}R\right)}{\sqrt{\frac{i\omega}{a_s}}RK_1\left(\sqrt{\frac{i\omega}{a_s}}R\right)+BiK_0\left(\sqrt{\frac{i\omega}{a_s}}R\right)} \qquad \text{(C6)}$$

Since the Kelvin function

$$K_0\left(u\sqrt{i}\right) = ker_0(u) + ikei_0(u) = N_0(u)e^{i\phi_0(u)},$$

$$e^{-\frac{\pi i}{2}}K_1\left(u\sqrt{i}\right) = ker_1(u) + ikei_1(u) = N_1(u)e^{i\phi_1(u)},$$

Substituting Equations (C6) to (C1), from the real part, $\Delta\tilde{T}_{in}$ can be expressed as:

$$\Delta\tilde{T}_{in} = [(1+\lambda A_1)^2 + (D+\lambda A_2)^2]^{-0.5}\Delta T_{out}cos(\omega t - \phi_{in-out}) \qquad \text{(C7)}$$

References

[1] "World Metro Figures 2018 – Statistic Brief" (PDF). Union Internationale des Transports Publics (UITP) (International Association of Public Transport). September 2018. p. 1. Archived from the original (PDF) on 26 October 2018. Retrieved 26 October 2018.

[2] 35 cities in China started rail transit, xinhuanet.com, (2019) [Online]. Available: http://www.xinhuanet.com/2019-04/03/c_1124323055.htm [Accessed: 29- Dec- 2020].

[3] F. Ampofo, G. Maidment, J. Missenden, Underground railway environment in the UK Part 1: Review of thermal comfort, Appl. Therm. Eng. 24 (2004) 611-631.

[4] M.J. Gilbey, S. Duffy, J.A. Thompson, The potential for heat recovery from London underground stations and tunnels, In Proceedings of the CIBSE Technical Symposium, Leicester, UK. 2011.

[5] A. Mortada, R. Choudhary, K. Soga, Thermal modelling and parametric analysis of underground rail systems, Energy Procedia, 78 (2015) 2262-2267.

[6] K. Jenkins, M. Gilbey, J. Hall, V. Glenis, C. Kilsby, Implications of climate change for thermal discomfort on underground railways, Transport. Res. D, 30 (2014) 1-9.

[7] Transport for London, London Underground Average Monthly Temperatures, (2018) [online]. Available: https://data.london.gov.uk/dataset/london-underground-average-monthly-temperatures [Accessed: 13- Jan- 2021].

[8] J.A. Thompson, G.G. Maidment, J.P. Missenden, F. Ampofo, Evaluation of underground railway networks operating sustainable cooling systems, Engineering the Future CIBSE, London, UK, 2006.

[9] Y. Zhang, X.F. Li, Response-surface-model based on influencing factor analysis of subway tunnel temperature, Build. Environ. 160 (2019) 106140.

[10] Griffiths, E. “Baking Hot at Baker Street.” Internet, London, (2006) [Online]. Available: http://news.bbc.co.uk/1/hi/england/london/5191604.stm [Accessed: 29- Dec- 2020].

[11] M. J. Gong, Subway tunnel temperature characteristics and its impact on the site environment, Master of Chongqing University, 2014.

[12] F. Ampofo, G. Maidment, J. Missenden, Underground railway environment in the UK Part 1: Review of thermal comfort, Appl. Therm. Eng. 24 (2004) 611-631.

[13] Y. Zhang, X. F. Li, Monitoring and analysis of subway tunnel thermal environment: A case study in Guangzhou, China, Sustain. Cities Soc. 55 (2020) 102057.

[14] Y. Wang, X.F. Li, STESS: Subway thermal environment simulation software, Sustain. Cities Soc. 38 (2018) 98-108.

[15] M. T. Ke, T. C. Cheng, W. P. Wang, Numerical simulation for optimizing the design of subway environmental control system, Build. Environ. 37 (2002) 1139-1152.

[16] A. Mortada, R. Choudhary, K. Soga, Multi-dimensional simulation of underground subway spaces coupled with geo-energy systems, J. Build. Perform. Simu. 11 (2018) 517-537.

[17] F. E. Camelli, G. Byrne, Rainald Löhner, Modeling subway air flow using CFD, Tunn. Undergr. Space Technol. 43 (2014) 20-31.

[18] C. F. Du, M. L. Bian, Numerical simulation of fluid solid coupling heat transfer in tunnel, Case Stud. Therm. Eng. 12 (2018) 117-125.

[19] Y. Zhang, X.F. Li, Heat transfer formalism using GFM and FEM in underground tunnels, Build. Environ. 143 (2018) 717-726.

[20] G. P. Dai, A. Vardy, Tunnel temperature control by ventilation, In Proceedings of the International Symposium on Aero Dynamics and Ventilation of Vehicle Tunnels, Liverpool, UK. 1994.

[21] D. Yang, J.P. Zhang, Theoretical assessment of the combined effects of building thermal mass and earth-air-tube ventilation on the indoor thermal environment, Energy Build. 81 (2014) 182-199.

[22] D. Yang, J. P. Zhang, Analysis and experiments on the periodically fluctuating air temperature in a building with earth-air tube ventilation, Build. Environ. 85 (2015) 29-39.

[23] F.X. Niu, Y. B. Yu, D. H. Yu, et al., Heat and mass transfer performance analysis and cooling capacity prediction of earth to air heat exchanger, Appl. Energy. 137 (2015) 211-221.

[24] X.C. Liu, Y. M. Xiao, K. Inthavong, et al., A fast and simple numerical model for a deeply buried underground tunnel in heating cooling applications, Appl. Therm. Eng. 62 (2014) 545-552.

[25] X.H. Zhou, Y.H. Zeng, L. Fan, Temperature field analysis of a cold-region railway tunnel considering mechanical and train-induced ventilation effects. Appl. Therm. Eng. 100 (2016) 114-124.

[26] Y.P. Yuan, X.K. Gao, H.W. Wu, et al., Coupled cooling method and application of latent heat thermal energy storage combined with pre-cooling of envelope: Method and model development, Energy. 119 (2017) 817-833.

[27] J. Yam, Y.G. Li, Zouhuan Zheng, Nonlinear coupling between thermal mass and natural ventilation in buildings, Heat and Mass Transf. 46 (2003) 1251-1264.

[28] L.N. Yang, Y.G. Li, Cooling load reduction by using thermal mass and night ventilation, Energy Build. 40 (2008) 2052-2058.

[29] J.L. Zhou, G.Q. Zhang, Y.L. Lin, Y.G. Li, Coupling of thermal mass and natural ventilation in buildings, Energy Build. 40 (2008) 979-986.

[30] Y.G. Li, J. Tam, Designing thermal mass in naturally ventilated buildings, Int. J. Vent. 2 (2003) 313-324.

[31] P.Z. Ma, L.S. Wang, Effective heat capacity of interior planar thermal mass (iPTM) subject to periodic heating and cooling, Energy Build. 47 (2012) 44-52.

[32] P.Z. Ma, L.S. Wang, Effective heat capacity of exterior planar thermal mass (ePTM) subject to periodic heating and cooling, Energy Build. 47 (2012) 394-401.

[33] Y. H. Zeng, L. L. Tao, X. Q. Ye, X. H. Zhou, Y. Fang, L. Fan, X. R. Liu, Z. X. Yang, Temperature reduction for extra-long railway tunnel with high geo-temperature by longitudinal ventilation, Tunn. Undergr. Sp. Tech. 99 (2020) 103381.

[34] H. Barrow, C. W. Pope, Theoretical global energy analysis for a railway tunnel and its environment, with special reference to periodic temperature change, Aerodynamics and Ventilation of Vehicle Tunnels. (1991) 267-280.

[35] S. Sadokierski, J.L. Thiffeault, Heat Transfer in Underground Rail Tunnels, eprint arxiv: 0709.1748, 2008.

[36] J. P. Holman, Heat Transfer, China Machine Press. 2011.

[37] J.M. Holford, A.W. Woods, On the thermal buffering of naturally ventilated buildings through internal thermal mass, J. Fluid Mech. 580 (2007) 3-29.

[38] A. Revesz, I. Chaer, J. Thompson, et al., Ground source heat pumps and their interactions with underground railway tunnels in an urban environment: A review, Appl. Therm. Eng. 93 (2016) 147-154.

[39] A. Revesz, I. Chaer, J. Thompson, M. Mavroulidou, M. Gunn, G. Maidment, Modelling of heat energy recovery potential from underground railways with nearby vertical ground heat exchangers in an urban environment, Appl. Therm. Eng. 147 (2019) 1059-1069.

[40] X. Y. Tan, W. Z. Chen, L. Y. Wang, J. P. Yang, The impact of uneven temperature distribution on stability of concrete structures using data analysis and numerical approach, Adv. Struct. Eng. 24 (2021) 279-290.

[41] A. Bidarmaghz, R. Choudhary, K. Soga, R. L. Terrington, H. Kessler, S. Thorpe, Large-scale urban underground hydro-thermal modelling – A case study of the Royal Borough of Kensington and Chelsea, London, Sci. Total. Environ. 700 (2020) 134955.

[42] F. Ampofo, G. Maidment, J. Missenden, Underground railway environment in the UK Part 3: Methods of delivering cooling, Appl. Therm. Eng. 24 (2004) 647-659.

[43] J. A. Thompson, G.G. Maidment, J.F. Missenden, Modelling low-energy cooling strategies for underground railways, Appl. Energy. 83 (2006) 1152-1162.

[44] J.A. Thompson, G.G. Maidment, J.F. Missenden, F. Ampofo, Geothermal cooling through enhancement of the natural heat sink effect – proof of concept, Exp. Therm. Fluid Sci. 31 (2007) 551-558.

[45] United States Department of Transportation, Subway Environmental Design Handbook Volume I Principles and Applications, 1976.

[46] F. Ampofo, G. Maidment, J. Missenden, Underground railway environment in the UK Part 2: Investigation of heat load, Appl. Therm. Eng. 24 (2004) 633-645.

[47] Y. J. Chai, T. T. Sun, H. T. Han, et al., Modularly design for waste heat recovery system in subway based on air source heat pump, Procedia Eng. 205 (2017) 273-280.

[48] K. Ninikas, N. Hytiris, R. Emmanuel, et al., Heat recovery from air in underground transport tunnels, Renew. Energy. 96 (2016) 843-849.

[49] G. Davies, N. Boot-Handford, D. Curry, W. Dennis, A. Ajileye, A. Revesz, G. Maidment, Combining cooling of underground railways with heat recovery and reuse, Sustain. Cities Soc. 45 (2019) 543-552.

[50] Energy Plus, Weather Data by Location, Weather Data Download – London Gatwick 037760 (IWEC), (2019) [Online]. Available: https://energyplus.net/weather [Accessed: 29-Dec- 2020].

[51] H.S. Carslaw, J.C. Jaeger, Conduction of Heat in Solids, Clarendon Press. 1959.